The small molecule CBR-5884 inhibits the *Candida albicans* phosphatidylserine synthase

Yue Zhou[1], Gregory A. Phelps[2, 3], Mikayla M. Mangrum[1], Jemma McLeish[1], Elise K. Phillips[1], Jinchao Lou[4], Christelle F. Ancajas[4], Jeffrey M. Rybak[5], Peter M. Oelkers[6], Richard E. Lee[2], Michael D. Best[4], and Todd B. Reynolds[1*]

1. Department of Microbiology, University of Tennessee, Knoxville, USA
2. Department of Chemical Biology & Therapeutics, St. Jude Children's Research Hospital, Memphis, USA
3. Graduate School of Biomedical Sciences, St. Jude Children's Research Hospital, Memphis, USA
4. Department of Chemistry, University of Tennessee, Knoxville, USA
5. Department of Pharmacy and Pharmaceutical Sciences, St. Jude Children's Research Hospital, Memphis, USA
6. Department of Natural Sciences, University of Michigan-Dearborn, Dearborn, MI, USA

*Corresponding author: treynol6@utk.edu

Running title: CBR-5884 inhibits *C. albicans* phosphatidylserine synthase

Abstract (241 words)

Systemic infections by *Candida spp.* are associated with high mortality rates, partly due to limitations in current antifungals, highlighting the need for novel drugs and drug targets. The fungal phosphatidylserine synthase, Cho1, from *Candida albicans* is a logical antifungal drug target due to its importance in virulence, absence in the host and conservation among fungal pathogens. Inhibitors of Cho1 could serve as lead compounds for drug development, so we developed a target-based screen for inhibitors of purified Cho1. This enzyme condenses serine and cytidyldiphosphate-diacylglycerol (CDP-DAG) into phosphatidylserine (PS) and releases cytidylmonophosphate (CMP). Accordingly, we developed an *in vitro* nucleotidase-coupled malachite green-based high throughput assay for purified *C. albicans* Cho1 that monitors CMP production as a proxy for PS synthesis. Over 7,300 molecules curated from repurposing chemical libraries were interrogated in primary and dose-responsivity assays using this platform. The screen had a promising average Z' score of ~0.8, and seven compounds were identified that inhibit Cho1. Three of these, ebselen, LOC14, and CBR-5884, exhibited antifungal effects against *C. albicans* cells, with fungicidal inhibition by ebselen and fungistatic inhibition by LOC14 and CBR-5884. Only CBR-5884 showed evidence of disrupting *in vivo* Cho1 function by inducing phenotypes consistent with the *cho1*ΔΔ mutant, including a reduction of cellular PS levels. Kinetics curves and computational docking indicate that CBR-5884 competes with serine for binding to Cho1 with a K_i of 1,550 ± 245.6 nM. Thus, this compound has the potential for development into an antifungal compound.

Importance (149 words)

Fungal phosphatidylserine synthase (Cho1) is a logical antifungal target due to its crucial role in the virulence and viability of various fungal pathogens, and since it is absent in humans, drugs targeted at Cho1 are less likely to cause toxicity in patients. Using *Candida albicans* Cho1 as a model, there have been two unsuccessful attempts to discover inhibitors for Cho1 homologs in whole cell screens prior to this study. The compounds identified in these attempts do not act directly on the protein, resulting in the absence of known Cho1 inhibitors. The significance of our research is that we developed a high-throughput target-based assay and identified the first Cho1 inhibitor, CBR-5884, which acts both on the purified protein and its function in the cell. This molecule acts as a competitive inhibitor with a K_i value of 1,550 ± 245.6 nM, and thus has the potential for development into a new class of antifungals targeting PS synthase.

Introduction

Candida species are the most commonly isolated fungal pathogens of humans (1, 2). *Candida* has been associated with mucosal infections, such as vulvovaginal infections in 51% of women or oropharyngeal infections in 27% of HIV+ patients, even when on anti-retroviral (ART) therapy (3, 4). In addition, these species are responsible for ~27% of bloodstream infections associated with a central line (1, 2, 5). *Candida* bloodstream infections pose a considerable threat to public health, with a mortality rate of approximately 40% (1, 2, 6, 7). *Candida albicans* is the most commonly isolated species within the *Candida* genus (1, 2, 8). Currently, there are only three classes of antifungal drugs in common use (azoles, polyenes, and echinocandins) for treating systemic *Candida* infections. However, their effectiveness is hindered by rising drug resistance to azoles and echinocandins and the toxicity profile of the polyene amphotericin B (9-13). Therefore, there is a pressing need to develop novel antifungal drugs.

Central in the phospholipid synthetic pathway in fungi is the phosphatidylserine (PS) synthase reaction (CDP-diacylglycerol—serine O-phosphatidyltransferase; EC 2.7.8.8) mediated by Cho1. This enzyme has been identified as a potential drug target due to the observations that [i] disruption of Cho1 in *C. albicans* prevents this fungus from causing disease in mouse models of systemic or oral infection (14, 15), and this enzyme is also crucial for the growth of the major fungal pathogen *Cryptococcus neoformans* (16); [ii] Cho1 is not present in mammals, indicating that specific inhibitors targeting this enzyme should not have toxic effects on humans (17), and [iii] *CHO1* is highly conserved across various fungal species, suggesting that inhibitors of this enzyme

would have broad spectrum anti-fungal effects (16, 17). Hence, inhibitors of Cho1 would be excellent lead compounds for antifungal drug development.

The fungal Cho1 enzyme was first characterized in the yeast *Saccharomyces cerevisiae*. This included descriptions of cellular localization in the endoplasmic reticulum and mitochondrial outer membranes (18-20), activity regulation (21-23) and protein purification (24, 25). Cho1 catalyzes the formation of PS from cytidyldiphosphate-diacylglycerol (CDP-DAG) and L-serine, and it belongs to the CDP-alcohol phosphatidyltransferase (CDP-AP) protein family. The CDP-AP proteins employ the highly conserved CDP-alcohol phosphotransferase (CAPT) motif, D-$(X)_2$-D-G-$(X)_2$-A-R-$(X)_2$-N-$(X)_5$-G-$(X)_2$-L-D-$(X)_3$-D, to bind CDP-linked molecules and facilitate the formation of a phosphodiester bond between the CDP-linked molecule and another small alcohol (16, 26-30), specifically CDP-DAG and serine for Cho1. However, it is important to note that the binding pocket for serine, unlike the CAPT motif, is not conserved among CDP-AP proteins. Previous studies have identified and characterized several crucial residues within the CAPT motif and the putative serine-binding site of *C. albicans* Cho1 through alanine scanning mutagenesis (26, 31). Additionally, valuable insights have been provided into the serine-binding pocket from the atomic structure of the PS synthase from the archaean *Methanocaldococcus jannaschii* (32). Differences between the *M. jannaschii* PS synthase and *C. albicans* Cho1 are apparent by the presence of differing numbers of transmembrane domains, oligomeric states, and there are specific residues in *C. albicans* Cho1 that play important roles, but the roles of corresponding residues in *M. jannaschii* PS synthase are unclear (26, 32).

Besides the characterization of the substrate-binding residues, *C. albicans* Cho1 has also been solubilized and purified as a hexameric protein (33), distinct from all the CDP-AP enzymes with solved structures (30, 32, 34-40), which are dimers. The hexameric *C. albicans* Cho1 can be separated into a trimer of stable dimers, indicating the hexamer might be [i] an early oligomer state, since Cho1 was solubilized from the early-to-mid log phase of *C. albicans* or [ii] species-specific (33). Furthermore, purified Cho1 enzyme was optimized for activity and was shown to have a K_m for CDP-DAG of 72.20 μM with a V_{max} of 0.079 nmol/(μg*min) while exhibiting a sigmoidal kinetic curve for its other substrate serine, indicating cooperative binding (33). This sigmoidal kinetic could potentially reconcile the contradicting high and low K_m values reported previously for *S. cerevisiae* PS synthase (22, 25, 41-43). The mechanism underlying the cooperative binding of serine is currently unknown.

Rational drug design is one way to discover compounds to a drug target protein. This can be achieved through either ligand-based or structure-based design methods (44). However, since there is a scarcity of known Cho1 ligands, and the atomic structure of *C. albicans* Cho1 has not yet been solved, employing rational drug design to identify Cho1-specific inhibitors is challenging. On the contrary, small molecule screening is an alternative way to identify inhibitors to Cho1 independent of structural information. Two whole-cell screens have been carried out to identify Cho1 inhibitors, but neither has been successful (45, 46). One identified the compound SB-224289, but it was discovered that SB-224289 only affects Cho1-associated physiological pathways (45). The other screen identified bleomycin, but this again impacts phospholipid related physiologies rather than Cho1 itself (46). Thus, to carry out identification of a Cho1 inhibitor, a target-based

screen was developed. This approach is enabled by the purification of Cho1, and is favorable because molecules identified will show direct inhibition of the target. Potential issues such as the cellular entry of molecules identified from target-based screening can be resolved later through medicinal chemistry approaches.

Cho1 activity has been measured in crude membrane preps (26, 31, 45, 47) and for the purified form (33, 48) using a radioactive substrate. However, that methodology is not practical for a high throughput screen. Here, we have adapted a non-radioactive assay with an easy setup and colorimetric readout (49), which detects the byproduct cytidine monophosphate (CMP) released from Cho1, to measure its activity in the presence of screening molecules. Using this assay, approximately 7,300 molecules were interrogated in a primary screen from a set of curated repurposing libraries to reveal one compound, CBR-5884, that stood out, as it displayed an inhibitory effect on Cho1 both *in vitro* and in live *C. albicans* cells.

Results

A malachite-green-based nucleotidase-coupled assay was used to screen for inhibitors of purified Cho1 protein

A expression cassette plasmid carrying the strong, constitutive promoter for translational elongation factor 1 (P_{TEF1}) fused upstream of the 8x-histindine tagged *C. albicans CHO1* gene was integrated into the genome at the *TEF1* locus to ensure a strong and stable expression level (50). Then, Cho1 was solubilized and purified from the microsomal fraction of *Candida albicans* as described in the Materials and Methods section. A blue native PAGE indicated that the Cho1 protein was purified to relative

147 homogeneity as a hexameric form of ~180 kDa (Figure 1A), consistent with findings in
148 (33). The purified Cho1 was used for small molecule screening.

149 A malachite green-based nucleotidase-coupled assay was used to measure the PS
150 synthesis activity of Cho1 (Figure 1B). Cho1 catalyzes the production of PS and
151 cytidylmonophosphate (CMP) from CDP-DAG and serine, where CMP can then be
152 recognized and cleaved by the nucleotidase CD73 to release inorganic phosphate, which
153 is subsequently detected by malachite green. To test whether this malachite green-based
154 assay can reflect Cho1 activity, a time-course test was performed with a fixed amount of
155 purified Cho1 in the presence of substrates (Figure 1C). The OD_{620} signal increased as
156 the reaction proceeded until it plateaued at 200 min, indicating that the assay is suitably
157 dynamic to probe Cho1 activity. Based on this data, a fixed time of 180 minutes was
158 chosen for the screen.

159 As no effective inhibitors of Cho1 have been identified to date, a highly potent
160 and selective inhibitor of the second step of the assay (nucleotidase CD73) was examined
161 as a positive control (51). This compound, AB-680, exhibited an IC_{50} value of 1.82 nM in
162 the malachite-green assay (Figure S1A). A concentration of 1 μM AB-680 was used in
163 the screen, and was compared to DMSO and no protein wells, which served as negative
164 controls. Reactions with AB-680 showed similar color as the no protein control in the
165 384-well plate (Figure 1D), and the measured OD_{620} signal was four-fold less in the
166 presence of the AB-680 (Figure 1E). Thus, AB-680 can be used as a positive control for
167 identifying inhibitors in the primary screen. In order to eliminate false positives that are
168 actually inhibiting the nucleotidase CD73, a counter-screening method was developed. In

this method, Cho1 was substituted with CMP, while CD73 remained included to identify any compounds that directly inhibit the nucleotidase instead of Cho1.

Seven Cho1-specific inhibitors were identified from the high throughput small molecule screen

The screen interrogated 7,307 molecules from three curated repurposing libraries in the primary screen and counter screen (which were run concurrently) at a final concentration of 100 μM each (Figure 2A). The primary screen had an average Z' score of ~0.8 (Figure S1B), indicating a good signal to noise ratio (52). To prioritize hit compounds and eliminate false positives, % Δinhibition (Figure 2B) was calculated by subtracting the % inhibition from the counter screen (Figure S1D) from that of the primary screen (Figure S1C) for each molecule. All compounds from the >80% Δinhibition population and selected molecules with limited structural liabilities from the 50-80% Δinhibition population (for a total of 82 molecules) were advanced for dose-response assessment using the same screening platform, which once again yielded results of high quality (Z' of 0.83; Figure S1E). Compounds exerting dose-dependent activity were then further triaged by manual inspection to exclude pan assay interference compounds (PAINS), which tend to react nonspecifically with numerous biological targets (53). Finally, seven molecules exerting IC_{50} values ≤ 76 μM were identified, of which CBR-5884, ML-345, ebselen and tideglusib were the most potent, possessing $IC_{50} \leq 20$ μM (Figure 2C). These molecules, in addition to avasimibe and LOC14 were selected for further investigation. The TC-N 22A molecule was not easily available and was not pursued.

Ebselen, LOC14 and CBR-5884 showed inhibitory effects on *C. albicans* cells

To further validate the inhibitory effects of the six molecules on Cho1, a radioactive PS synthase assay was conducted on Cho1 in the presence of these compounds. Unlike the malachite green-based assay, the radioactive PS synthase assay directly measures the incorporation of L-[^{3}H]-serine into PS in the lipid phase (26, 33, 47). The radioactive PS synthase assay was performed on purified Cho1 in the presence of the six compounds at 100 μM, and all six molecules were shown to totally inhibit Cho1 (Figure 2D), consistent with the screening results.

We then tested the effects of the six compounds on live cells by determining the minimal inhibitory concentrations (MICs) of these compounds. Following the standard Clinical & Lab Standards Institute (CLSI) MIC broth microdilution methods, wildtype *C. albicans* strain SC5314 was grown with avasimibe, CBR-5884, tideglusib, ebselen, ML-345 and LOC14 in RPMI MOPS medium (pH=7.0) or alternatively in minimal medium or minimal medium with HEPES (pH=7.0) at 37°C for 48 hours, along with a *cho1*ΔΔ strain as a control (Figure 3A-C). The concentration of the compounds was varied from 0.5 to 250 μM. Avasimibe, tideglusib and CBR-5884 precipitated at high concentrations, indicating a low solubility (Figure S2A). Among all compounds, avasimibe and tideglusib did not affect cell growth in all three different media, even at 250 μM, indicating they do not have an inhibitory effect on *C. albicans* cells under our assay conditions (Figure 3A-C). ML-345 only inhibited cell growth in RPMI MOPS medium with an MIC of 31.3 μM, and had no effect on cells grown in the minimal media.

213 Ebselen, LOC14 and CBR-5884, on the contrary, stopped cell growth at different
214 concentrations in all three media (Figure 3A-D), with MICs ranging between 7.8-31.3
215 μM. This is consistent with the radioactive PS synthase assay done on the crude
216 membrane containing Cho1, in which only ebselen, CBR-5884 and LOC14 decreased PS
217 production in the native crude membranes (Figure S3). Specific MIC values are
218 summarized in Figure 3D for all the compounds.

219 Furthermore, there are no current reports on the antifungal effects of LOC14 and
220 CBR-5884. To rule out the possibility that their inhibition is strain-specific, we treated
221 four additional *C. albicans* wildtype strains—GDH2346 (54), 3153A (55), and two
222 clinical isolates TFPY412 and TFPY2307—with LOC14 and CBR-5884. Tests were
223 done in RPMI MOPS (pH=7.0) medium at 37°C for 48 hours following the CLSI MIC
224 broth microdilution protocol, and a *cho1ΔΔ* strain was included as a control (Figure 3E,
225 F). As shown, all strains were inhibited by LOC14 and CBR-5884 at varying
226 concentrations, indicating their inhibition is not specific to certain strains.

227

228 **The inhibitory effect of CBR-5884 can be rescued by ethanolamine supplementation**

229 The antifungal effects of ebselen, LOC14 and CBR-5884 on live cells were
230 further evaluated by plate assays and growth curves. Firstly, we tried to determine if the
231 inhibitory effects of these compounds were fungistatic or fungicidal. It should be
232 highlighted that in contrast to the MIC assays, the plate assays and growth curve analyses
233 necessitated a greater initial inoculum (OD_{600} of 0.05 as opposed to 0.00004) for
234 detection. Additionally, a reduced incubation temperature of 30°C instead of 37°C was

235 required to inhibit the hyphal formation, which in turn required the adjustment of
236 compound concentrations used. For this, wildtype *C. albicans* strain SC5314 was grown
237 with varying concentrations of ebselen, LOC14 and CBR-5884 in minimal media at 30°C
238 for 24 hours, along with a *cho1*ΔΔ strain as a control. Under this condition, ebselen
239 suppressed cell growth at concentrations from 15.9 μM to 31.8 μM, LOC14 showed
240 inhibition within the range of 250 μM to 500 μM, and CBR-5884 was effective between
241 125 μM and 250 μM, as reflected by both the decreased growth in the 96-well plates and
242 reduced cell density in the microscope images in the upper concentrations (Figure S4). To
243 further determine the optimized inhibition concentrations and whether the inhibition is
244 fungistatic or fungicidal, wildtype *C. abicans* SC5314 was then incubated with ebselen,
245 LOC14 and CBR-5884 in a dosage series with 10 μM increments within the inhibition
246 range determined above, and colony forming units (CFUs) were counted after 24-hour
247 incubation. Ebselen showed no colonies after incubation at 30 μM, which is consistent
248 with a fungicidal effect (Figure 4A). In contrast, cells incubated with 430 μM LOC14 and
249 170 μM CBR-5884 exhibited similar CFUs as the pre-incubation, indicative of a
250 fungistatic effect (Figure 4B&C).

251 Next, we determined if the impacts of ebselen, LOC14 and CBR-5884 on cells
252 were consistent with perturbed Cho1 function. Cho1 synthesizes PS via the *de novo*
253 pathway, the lipid precursor for making essential phospholipid phosphatidylethanolamine
254 (PE). When Cho1 is inhibited, growth can only resume, albeit more slowly, if the
255 organism is able to make PE from ethanolamine acquired from the medium via the
256 salvage (Kennedy) pathway (14, 26). Thus, ethanolamine-dependent growth in minimal
257 media is a characteristic phenotype of PS synthesis loss. Thus, the growth inhibition

assay was repeated at the optimized drug concentrations in minimal medium supplemented with 1mM ethanolamine, and an increase in the CFUs in the presence of ethanolamine indicates an inhibition on Cho1 function. Although ethanolamine did not rescue cells with ebselen or LOC14, cells treated with the ≥170μM CBR-5884 generated significantly higher CFUs upon addition of ethanolamine (Figure 4A-C). This result suggests that the inhibitory effect of ebselen and LOC14 on the cells are not solely caused by Cho1 inhibition, while CBR-5884 is more directly targeting Cho1.

To gain insight into the dynamic, inhibitory properties of these molecules, growth curves were determined with wildtype cells grown in the minimal media ± ethanolamine, in the presence of CBR-5884 or LOC14. Ebselen was not pursued in the growth curve assay due to its fungicidal effect. The *cho1*ΔΔ strain was used as a control for loss of Cho1 activity. Given that CBR-5884 is a selective inhibitor of phosphoglycerate dehydrogenase that is involved in *de novo* serine synthesis in cancer cells (56), and to make sure that the growth perturbation is not due to serine starvation, 5 mM serine was also added to the media ± ethanolamine. As shown in Figure 4D, cells grown in media + ethanolamine and + ethanolamine/serine grew similarly, while those grown in minimal media and minimal media + serine had similarly reduced growth. This suggests that serine did not help the cells recover from the inhibition from CBR-5884, which likely indicates [i] CBR-5884 does not target *C.albicans* phosphoglycerate dehydrogenase or [ii] the CBR-5884 inhibition of *C. albicans* phosphoglycerate dehydrogenase is not the major cause of diminished growth. Cells with ethanolamine supplementation grew better than those in minimal media alone, especially from 12 to 24 hours, consistent with Figure 4C. Growth rates during log phase (Figure S2B) and lag phase duration (Figure S2C)

were estimated from the growth curves, and they showed that the addition of ethanolamine significantly increased the growth rate and decreased the lag time. All of these results again support the hypothesis that CBR-5884 targets Cho1 *in vivo*.

However, it was observed that the impact of CBR-5884 on cell growth was only temporary, with a delay lasting 12 hours. After this period, cells treated with CBR-5884 exhibited rapid growth, eventually matching the growth rate of the DMSO control group following a 24-hour incubation period (Figure 4D). This suggests that either (i) CBR-5884 lost its effect after 12 hours of agitation or (ii) that *C. albicans* cells acquire resistance to the compound within this timeframe. To disentangle these two possibilities, experiments were conducted where both CBR-5884 and DMSO were subjected to 12 hours of agitation at 30°C before being introduced to live cells. The growth of these cells was monitored over the next 14 hours, with an OD_{600} measurement every 2 hours, to assess the persistence of CBR-5884's efficacy (Figure 4F); In the meantime, cells that had been grown in 170 μM CBR-5884 for 12 and 24 hours were transferred into fresh media containing new CBR-5884, which was allowed to grow for another 14 hours, to probe the rising of resistance (Figure 4G). In both experimental setups, cells grew slowly in the presence of CBR-5884 compound compared to DMSO control. This suggests (i) CBR-5884 maintains its stability and effectiveness under agitation for at least 12 hours, and (ii) the breakout growth in Figure 4D is not due to the rise of resistance to CBR-5884. One possible explanation could be that *C.albicans* cells metabolize the CBR-5884 compound, making it inactive after 12 hours and resulting in a surge in growth.

Furthermore, LOC14 was also subjected to growth curve determination but no cells grew, in the presence or absence of ethanolamine (Figure 4E). This corroborates

with Figure 4B that the inhibition by LOC14 is not acting solely on Cho1. Since the goal was a Cho1-specific inhibitor, ebselen and LOC14 were not pursued further.

CBR-5884 interferes with PS synthesis *in vivo*

It has been determined previously that deletion of Cho1 leads to increased exposure (unmasking) of cell wall β(1-3)-glucan, rendering cells more prone to be targeted by the immune system (14, 57). Here, we tested whether CBR-5884 could induce unmasking. Wildtype *C. albicans* cells were grown in rich medium (YPD) supplemented with DMSO or CBR-5884 for 30, 60 and 120 min, along with the *cho1*ΔΔ mutant control, and exposed β(1-3)-glucan was stained and visualized through confocal microscopy. The *cho1*ΔΔ strain exhibited increased unmasked foci, compared to the WT strain in DMSO, consistent with previous findings that disruption of Cho1 leads to increased unmasking (Figure 5A) (57). Similarly, CBR-5884 treatment showed increased unmasking after 30-min incubations, and the unmasking became more obvious at 60- and 120-min treatment. The mean fluorescence values confirmed that a 30-min CBR-5884 treatment is sufficient to induce significantly increased unmasking compared to wildtype *C. albicans*, and 120-min treatment could induce more unmasking than the *cho1*ΔΔ mutant (Figure 5B). This could be because CBR-5884 inhibition causes a sudden loss of Cho1 function that the cells have not yet adjusted to, whereas a *cho1*ΔΔ mutant has adjusted its metabolism to the loss of PS. Alternatively, it may indicate an off-target effect. It is also interesting to note that there are dark structures in the cells under bright field microscopy when treated with CBR-5884, which are absent in wildtype or *cho1*ΔΔ strains without CBR-5884. We currently cannot explain the identity or formation of these

structures, but speculate that they represent fragmented vacuoles that serve in detoxification (58).

In order to more directly measure the impact of CBR-5884 on PS synthesis *in vivo*, an assay for fluorescence-based labeling of PS via biorthogonal tagging using a clickable serine probe was utilized. This probe consists of a serine analogue carrying an azide tag for click chemistry, C-L-SerN_3. This probe has been demonstrated to be incorporated into live cell membranes by infiltrating lipid metabolism to produce azide-tagged PS analogues that can be post-labeled by click-tagging with fluorophores to localized/quantify PS in cells (59, 60). Wildtype *C. albicans* was grown in YPD to early log phase before C-L-SerN_3 was added, along with CBR-5884 or DMSO (Figure 5C). The *cho1*ΔΔ strain and no probe controls were also included for background fluorescence, and mean fluorescence of each group was quantified (Figure 5D). In the absence of CBR-5884, C-L-SerN_3 labels the cell membrane of wildtype *C. albicans* with stronger fluorescence compared to no probe or *cho1*ΔΔ strains (Figure 5C&5D), indicating C-L-SerN3 was converted into PS as previously described (59). However, in the presence of CBR-5884, the fluorescence is significantly diminished on the periphery of the cell (Figure 5C&D). This indicates that CBR-5884 inhibits *in vivo* PS production.

Finally, a direct biochemical test for PS levels was performed by thin layer chromatography (TLC) in cells treated with CBR-5884. Wildtype *C. albicans* and *cho1*ΔΔ strains were grown in the presence and absence of CBR-5884, and the four major phospholipid species are shown in Figure 5E and quantified in Figure 5F. Consistently, the relative PS level in wildtype *C. albicans* strain treated with CBR-5884 significantly dropped compared to the DMSO treatment (Figure 5E&5F), indicating that

CBR-5884 interferes with PS production. Interestingly, the relative PE levels also significantly decreased in strains treated with CBR-5884, especially in the *cho1*ΔΔ strain without PS as a precursor (Figure 5E&5F). This potentially indicates that CBR-5884 may independently impact PE production.

CBR-5884 acts as a competitive inhibitor that occupies the serine binding site of Cho1

To determine whether CBR-5884 is an irreversible inhibitor, which forms covalent bonds with Cho1, the compound was pre-incubated with purified Cho1 protein for 2 hours, followed by a buffer exchange and washout before the reaction (Figure 6A). The absence of inhibition after preincubation and washout suggests that CBR-5884 does not inhibit the enzyme covalently. To investigate the molecular mechanism by which CBR-5884 inhibits Cho1, purified Cho1 specific activity was assayed with varying concentrations of serine and CDP-DAG in the presence of CBR-5884. Serine was varied from 4 to 32 mM, CDP-DAG was kept at 200 μM, and several concentrations of CBR-5884 were tested (Figure 6B). The pattern of inhibition more closely fits with competitive inhibition and a low K_i value of 1,550 ± 245.6 nM. Next, serine was held at a sub-saturating concentration of 20 mM or a saturating concentration of 32 mM, and CDP-DAG was varied from 25 to 300μM. At the lower serine concentration, the inhibition of CBR-5884 on Cho1 activity was observed (Figure 6C), but the inhibition was overcome under saturating serine concentrations (Figure 6D). These results suggest that CBR-5884 inhibits Cho1 by competing for serine and can be outcompeted with a high serine concentration. It is interesting that CDP-DAG inhibits Cho1 activity at high

concentrations, especially in the presence of CBR-5884 (Figure 6C). This substrate inhibition from CDP-DAG has been reported previously (22, 61).

To gather more insight for the serine competition, we computationally docked CBR-5884 into the active site of *C. albicans* Cho1. Since fungal PS synthases follow the ordered sequential bi-bi reaction mechanism where Cho1 binds CDP-DAG before serine for catalysis (25), we first generated a predicted CDP-DAG-bound *C. albicans* Cho1 structure by superposing the *C. albicans* Cho1 AlphaFold model on the CDP-DAG-bound PS synthase from *Methanocaldococcus jannaschii* (PDB: 7B1L) (Figure S5A) (32). The CDP-alcohol phosphotransferase (CAPT) binding motif, which is known to bind CDP-DAG, is conserved and aligned between the *C. albicans* Cho1 and *M. jannaschii* PS synthase structures, so we hypothesized that the CDP-DAG from *M. jannaschii* PS synthase interacts with *C. albicans* Cho1 in a very similarly manner, and thus is incorporated in the *C. albicans* Cho1 model for docking. Next, we simulated and combined all the possible active site pockets from the CDP-DAG-bound *C. albicans* Cho1, and docked CBR-5884 and L-serine into these possible sites (Figure S5B). A total of 20,000 initial poses of CBR-5884 and serine were generated and then refined to the 5 top poses with the highest docking scores (Figure 6E). All five CBR-5884 poses have overlap with the serine poses, with a higher docking score of -11.48 ± 0.12 kcal/mol compared to the serine docking score of -6.72 ± 0.08 kcal/mol. This corroborates the low K_i value and suggests that CBR-5884 likely competes with serine to occupy the serine binding pocket in Cho1. From this, we generated a working model for CBR-5884 inhibition (Figure 6F). Following the first step in the sequential bi-bi reaction where Cho1 binds CDP-DAG, either CBR-5884 or serine can dock into the active site. The

catalysis will occur if serine enters, and will not if CBR-5884 occupies the site. Since CBR-5884 is favored by Cho1, serine can only outcompete CBR-5884 at a high concentration.

Discussion

Here, we adapted a malachite green-based nucleotidase-coupled assay to screen for and identify inhibitors targeting *C. albicans* Cho1 (49). Since the amount of phosphate released is directly proportional to the CMP, and thus PS, produced in the reaction, this method can be used to measure Cho1 activity in real time (Figure 1C). It is worth mentioning that besides CMP, the nucleotidase CD73 is known to cleave AMP to release phosphate in various studies (62-64), and given that this assay is suitable for 384-well plates or even 1536-well plates, it may potentially be applied to any enzyme producing AMP/CMP.

Ebselen, LOC14 and CBR-5884 stood out among seven Cho1-specific inhibitors due to their inhibitory effects on the *C. albicans* cell growth (Figure 3). Ebselen is an organo-selenium compound originally developed as a glutathione peroxidase mimic that acts on the cholesterol ester hydroperoxides and phospholipid hydroperoxides (65), and it has garnered significant attention in recent years due to its diverse therapeutic applications due to its anti-inflammatory, antioxidant and anticancer activity (66-71). In addition, ebselen has exhibited notable *in vitro* and *in vivo* antifungal activity against a range of fungal pathogens, including *Candida* spp., *Fusarium* spp., *Aspergillus fumigatus* and *Cryptococcus neoformans* (72-74). Studies have shown that ebselen effectively inhibits fungal growth by targeting many key enzymes (75-80). Here, we have

419 demonstrated again that ebselen inhibits wildtype *C. albicans* growth (Figure 3&4). The
420 inhibition of purified Cho1 by ebselen is potent, with an IC_{50} of 11.1 μM (Figure 2C), but
421 the inhibition on Cho1 is very likely not the main cause for ebselen's inhibition of *C.*
422 *albicans* growth, since ethanolamine cannot bypass the drug (Figure 4). Currently, we do
423 not know the mechanism of ebselen's inhibition on Cho1, but given the tendency for
424 ebselen to interact with cysteine residues (81), we hypothesize that ebselen might interact
425 with residue C182, located in the putative serine-binding site of Cho1 (26), thus
426 disrupting activity. Ebselen's promiscuous nature limits its clinical applicability.

427 Conversely, the antifungal effects of LOC14 and CBR-5884 have not been
428 studied. LOC14 is a potent, non-covalent and reversible inhibitor for protein disulfide
429 isomerase that has a neuroprotective effect in corticostriatal brain culture, and it was
430 shown that LOC14 was well tolerated at high dose of 20 mg/kg to C57BL/6j mice in the
431 *in vivo* pharmacokinetic study (82). In addition, LOC14 displayed promising effects
432 against Huntington's disease (83) and can be used in a new anti-influenza therapeutic
433 strategy (84). Here, we showed that LOC14 inhibits Cho1 activity (Figure 3), however,
434 the *in vivo* inhibition is not likely conveyed through Cho1 (Figure 4). In contrast, CBR-
435 5884 is an inhibitor of phosphoglycerate dehydrogenase, blocking *de novo* serine
436 synthesis in cells, and is selectively toxic to cancer cell lines with high serine biosynthetic
437 activity against melanoma and breast cancer lines (56). Here, CBR-5884 was shown to
438 not only inhibit purified Cho1 (Figure 2&6), but also inhibit live cell growth by acting on
439 the Cho1 *in vivo* (Figure 3-5). To our knowledge, this is the first report showing the
440 antifungal effects of LOC14 and CBR-5884.

441 CBR-5884 was then determined to be a competitive inhibitor of Cho1 with a K_i of
442 1550 ± 245.6 nM via kinetic analysis (Figure 6). Interestingly, in non-saturating serine
443 concentrations (Figure 6C), the kinetic curves decreased in height and shifted to the left
444 in the presence of increasing concentration of CBR-5884, indicating a decreasing K_m and
445 V_{max}, mimicking an uncompetitive inhibition where the inhibitor only binds to substrate-
446 bound enzyme complex and thus depletes its population. This suggests that CBR-5884 is
447 able to compete with serine by binding CDP-DAG-bound Cho1, and it cannot compete
448 with CDP-DAG to bind to empty Cho1. The V_{max} of Cho1 in this study is estimated to be
449 0.128 ± 0.029 nmol/(μg*min), which is close to 0.088 ± 0.007 nmol/(μg*min) as
450 described in (33). Also, it is worth mentioning that the curves where CDP-DAG was held
451 constant and serine was varied follow a sigmoidal shape, which is consistent with
452 previous finding that serine-binding may be cooperative (33), but the underlying
453 mechanism is not clear. One small discrepancy has to be pointed out that the K_{half} of
454 serine in this study is determined to be 17.08 ± 4.072 mM, which is four time higher than
455 the 4.17 ± 0.45 mM from (33). The increased K_{half} may be explained by the presence of
456 DMSO in this study, as DMSO has been shown to increase K_m in some enzymes (85-87).

457 CBR-5884 and serine were also docked onto the predicted CDP-DAG-bound
458 Cho1 structure, and CBR-5884 was found to overlap with serine in the pocket (Figure
459 6E). A detailed ligand interaction map has shown that CBR-5884 almost shielded the β-
460 phosphorus of the CDP-DAG where the nucleophilic attack occurs (30, 35), and also
461 some CBR-5884 poses directly interact with residues R186 and F190 in Cho1 (Figure
462 S6), which are part of the putative serine-binding site and are shown to be essential for
463 Cho1 activity (26). This indicates again that CBR-5884 inhibits Cho1 by competing with

serine. However, we acknowledge that the molecular docking results presented herein are based on a predicted protein model and are subject to the inherent limitations of *in silico* methods. Future experimental validation will be necessary to fully elucidate the molecular mechanisms behind the inhibition by CBR-5884.

Our data strongly suggest that CBR-5884 inhibits Cho1 *in vivo*, however, Cho1 may not be the only cellular target of CBR-5884. This compound causes cells to become more unmasked than the *cho1*ΔΔ mutant (Figure 5B). This could be due to sudden drop in PS caused by the compound compared with the *cho1*ΔΔ mutant, which has adjusted to the change. However, it could also be due to inhibition of another target. In addition, in TLC analysis, it was revealed that CBR-5884 decreased PS and also impacted relative PE levels similarly to that seen in a *cho1*ΔΔ mutant (Figure 5E&5F). However, the CBR-5884 compound caused a greater decrease in PE levels in the *cho1*ΔΔ mutant than that observed in wild-type or untreated *cho1*ΔΔ cells. The compound also decreases growth of the *cho1*ΔΔ strain in rich YPD media (Figure S7), suggesting that it has an additional target besides PS synthase. Since the *cho1*ΔΔ strain cannot use PS as the precursor to make PE, the PE is made primarily via the Kennedy pathway, which requires CDP-ethanolamine phosphotransferase (14, 88). Cho1 and CDP-ethanolamine phosphotransferase belong to the same protein family and both use the CDP-alcohol phosphotransferase (CAPT) binding motif (29, 89, 90), so it is possible that CBR-5884 also inhibits CDP-ethanolamine phosphotransferase activity. Interestingly, PI synthase also has the CAPT motif and binds CDP-DAG (91, 92), but the PI levels were not strongly affected (Figure 5E&F). Thus, the impact would be more specific to ethanolamine phosphotransferase in this case.

Moreover, this cross-reactivity could potentially be addressed by medicinal chemistry to synthesize analogs more specific for Cho1 and act at lower IC_{50}, which could decrease off-target effects and increase potency. Importantly, we have novel proof of principle for successful pharmacological inhibition of a uniquely fungal enzyme central to phospholipid metabolism. Future rational drug design study will optimize CBR-5884 to be more specific for Cho1, as well as increase the solubility and potency of the compound in live cells.

Materials and Methods

Strain construction and media

This study used a *C. albicans* strain derived from SC5314 that was disrupted for *CHO1*, but had the gene complemented back with an affinity-tagged version. This strain *cho1*ΔΔ P_{TEF1}-*CHO1-ENLYFQG-HAx3-HISx8*, was made in this study and used to solubilize and purify Cho1. This strain expressed a Hisx8-tagged Cho1 protein from a strong constitutive P_{TEF1} promoter. To create this strain, a plasmid was generated that carried the tagged *CHO1* gene. This plasmid had a hygromycin B resistance gene, *CaHygB*, as a selectable marker for transformations. To make the plasmid pKE333, first the *CaHygB* marker cassette was amplified from the *CaHygB*-flipper plasmid (93) using primers YZO113 & YZO114 having *NheI* and *MscI* cut site, respectively (Table 1). The *CaHygB* cassette was ligated into pKE4 plasmid (50) that had been digested with *NheI* and *MscI*, to create the plasmid pKE4 - *CaHygB* (pKE333). Then, the *CHO1-ENLYFQG-HAx3-HISx8* gene, with the 3'UTR region was amplified from pYZ79 (33) using primers YZO110 & YZO111 and ligated into pKE333 cut with *ClaI* and *MluI* to create the

plasmid pYZ107. Plasmid pYZ107 was linearized with *PmlI* restriction enzyme (within the P_{TEF1} sequence) and electroporated into the *cho1*ΔΔ strain (14). Transformants were selected on YPD plates containing 600 μg/ml hygromycin B. Colony PCR was performed on six candidates for each gene construct to ensure the successful integration under the P_{TEF1} promotor on the chromosomal DNA, and no spurious mutations occurred during the transformation. Media used in this study include YPD (1% yeast extract, 2% peptone, 2% dextrose), minimal medium (0.67% yeast nitrogen base W/O amino acids, 2% dextrose ± 1 mM ethanolamine ± 50 mM HEPES, pH 7.0, and RPMI + 20 mM MOPS pH 7.0).

Cell lysis, protein solubilization and purification

The *C. albicans* strain with His-tagged Cho1 expressed from P_{TEF1} was grown in YPD until the OD_{600} reached 7.0-8.0, then cells were lysed using a French press, as described in (47). Crude membranes were collected and solubilized with 1.5% digitonin as described in (33). His-tagged Cho1 was first purified via gravity affinity chromatography as describe in (33), and was further cleared by size exclusion chromatography (Superdex 200 10/300 GL column (Cytiva) attached to an NGC chromatography system Quest 10 plus (Bio-Rad)). The column was equilibrated with 1.5 column volumes of H_2O and 1.5 column volumes of elution buffer (50 mM Tris-HCl (pH=8.0) + 0.04% digitonin) with a flow rate of 0.5 mL/min. Samples loaded onto the above column consisted of a concentrated Cho1 eluted from affinity chromatography that was filtered through 0.22 μm filters that was then manually injected in the sample loop. The injected sample was eluted at a flow rate of 0.4 mL/min. Fractions containing Cho1 were pooled and subjected to AcTEV treatment, and then run through another round of

affinity chromatography to remove impurities as described in (33). The resulting sample was loaded and checked on the blue-native PAGE for purity, oligomer state and homogeneity.

High-throughput malachite green screen

The bioactives library was purchased from Selleck in 2014, and the remaining libraries (anti-infectives and mechanism of action libraries) were assembled from compounds available at the Chemical Biology and Therapeutics Department at St. Jude Children's Research Hospital. The anti-infectives library contains a curated list of antimicrobials and antiviral agents (94). The bioactive library has a compilation of compounds acquired from commercial sources and external academic collaborators. The mechanism of action set is a dynamic set of well-annotated compounds with comprehensive coverage of human targets and mechanisms of action (95). All compounds were dissolved in DMSO and 100 nL was transferred to a 384-well clear bottom plate (ThermoFisher Scientific, cat# 265203) using a Beckman Echo 650 acoustic liquid handler. Equal volumes of either the selective CD73 nucleotidase inhibitor AB680 at a final concentration of 1 μM (MedChemExpress, cat# HY-125286) or DMSO were used as positive and negative controls, respectively. A total of 30-35 ng of purified Cho1 protein was used in each reaction in 50 mM Tris-HCl (pH=8.0) for primary screening, combined with 100 μM CDP-DAG (Avanti, cat# 870510), 5 mM serine, 0.4 ng CD73 nucleotidase (R&D systems, cat# EA002), 1 mM $MnCl_2$, 0.1% APX-100 and 0.1% digitonin, in a total volume of 10 μL. Counter screen reactions were set up by replacing only the purified Cho1 with 150 μM CMP, with all other components remaining constant.

554 The 10 μL primary and counter screening reactions were delivered to each well of 384-
555 well assay plates containing pre-aliquoted compounds from the library using a Multidrop
556 Combi (ThermoFisher Scientific). This resulted in a DMSO concentration of 1%. After
557 media transfer, assay plates were incubated for 3 hours at 30 °C. Plates were then
558 removed and 32 μL of malachite green mixture (6 μL malachite A (2% (w/v) ammonium
559 molybdate and 20% (v/v) sulfuric acid in H_2O) + 20 μL H_2O + 6 μL malachite B (0.1%
560 (w/v) malachite green oxalate and 0.5% (w/v) polyvinyl alcohol in H_2O)) were added to
561 each well via a MultiDrop Combi and incubated for an additional 10 minutes at room
562 temperature. After incubation, plates were briefly centrifuged at 500 xg and absorbance at
563 620 nm was then measured using a Cytation7 plate reader (Biotek, Winooski, VT). Raw
564 absorbance values of the compounds were normalized to DMSO (0% inhibition) and
565 AB680 (100% inhibition) from both primary and counter screens, and % Δinhibition was
566 calculated by subtracting % inhibition measured in the primary screen from the %
567 inhibition measured in the counter screen. Z-factors for each plate were calculated using
568 the in-house program RISE (Robust Investigation of Screening Experiments). All non-
569 PAINs compounds that had >80% Δinhibition progressed to dose-response testing (82
570 total compounds). Dose-response experiments were performed in triplicate as described
571 above using a 10-point, threefold serial dilution with the top concentration for each
572 compound tested being 200 μM (Range: 0.010161-200 μM). The absorbance at 620 nm
573 was then measured using a PHERAstar FS multilabel reader (BMG, Cary, NC). Raw
574 values were once again normalized to DMSO (0% inhibition) and AB680 (100%
575 inhibition) and Z-factors for each plate were calculated using RISE. The concentration of
576 test compounds that inhibited Cho1 by 50% (IC_{50} value) as measured by the malachite

green assay was computed using nonlinear regression-based fitting of inhibition curves using [inhibitor] vs. response-variable slope model in GraphPad Prism version 9.5.0 (GraphPad Software, La Jolla California USA).

Assay for metabolic labeling of PS using probe C-L-SerN$_3$

The C-L-SerN$_3$ probe ((*S*)-1-((3-azidopropyl)amino)-3-hydroxy-1-oxopropan-2-aminium chloride) was synthesized as described in (59). Cells grown overnight in YPD were washed three times in H_2O and inoculated into minimal media at a starting OD600 of 0.05. Cells were shaken for 5 hours before 1.5 mM C-L-SerN$_3$ probe was added, along with 170 μM CBR-5884 or an equivalent volume of DMSO. Cells were then incubated for another 5 hours before being washed three times with H_2O, and 5% BSA in 1xPBS was used to treat cells for 20 min. The cells were then washed three times with 1xPBS, and then resuspended to OD_{600} of 0.6 in 1 mL PBS + 1 μM AZDye 488 DBCO (Click chemistry tools, cat# 1278-1). Cells were covered with aluminum foil and rocked for 1 hour, and the dye was removed by pelleting the cells at 5,000 xg followed by washing with shaking at 1,000 rpm three times in 1xPBS, and resuspended in 200 μL Fluoromount-G mounting medium (cat# 00-4958-02). For each treatment, 10 μL of cells were added to a glass slide and 3 μL fresh Fluoromount-G mounting medium was used to mix the sample. Then, a Leica SP8 white light laser confocal microscope was used for imaging. The samples were excited using light at a wavelength of 488 nm, and the resulting fluorescence was captured within the range of 498 to 550 nm using a HyD detector. The settings for laser strength, gain, and offset were maintained consistently throughout the experiment. Images of treated cells were taken after applying a zoom

599 factor of 3. A total of 40 cells from at least 10 images were used for the quantification in
600 ImageJ software.

601 **Fluorescence imaging of unmasked β(1-3)-glucan**

602 Wildtype and *cho1*ΔΔ cells were grown in YPD overnight (~16 hours), and back
603 diluted to fresh YPD with OD_{600} of ~0.1. The cells were then shaken at 225 rpm for 3
604 hours before 170 μM CBR-5884 or equivalent DMSO were added. The cells were further
605 shaken for 30, 60, 120 mins before staining with anti- β(1-3)-glucan antibody. The cells
606 were stained as previously described (57, 96) with the exception that goat anti-mouse
607 antibody conjugated to Alexa Fluor® 488 (Jackson ImmunoResearch) was used as the
608 secondary antibody. For imaging, *Candida* cells were resuspended in 200 μL of
609 Fluoromount-G mounting medium and visualized with a Leica SP8 white light laser
610 confocal microscope. The pictures were taken through Leica Application Suite X office
611 software.

612 **MIC plates tests and growth curves**

613 Minimum inhibitory concentration (MIC) was determined following Clinical &
614 Lab Standards Institute (CLSI) MIC broth microdilution protocol (Licensed to Todd
615 Reynolds, license # Ord-1138682) (97, 98). Briefly, stock solutions of different
616 compounds (purchased from MedChemExpress) were prepared at a concentration of 10
617 mM in DMSO and subsequently diluted as required in the same solvent. Wildtype *C.*
618 *albicans* strain SC5314, as well as four additional wildtype strains—GDH2346, 3153A,
619 TFPY412 and TFPY2307, were cultured overnight in YPD medium at 30°C, then washed

with water for three times and diluted to a concentration of 2×10^3 cells/mL (OD_{600}=0.00008) in one of the three media (Minimal medium, minimal medium buffered with 50 mM HEPES (pH=7.0) and RPMI MOPS (pH=7.0)). The *cho1*ΔΔ strain was also include as a control. A volume of 100 μL from each cell suspension was dispensed into the wells of a flat-bottom 96-well plate. An additional 100 μL of corresponding medium, containing twice the final desired concentration of each drug, was added to each well, leading to a final initial inoculum of 2×103 cells/mL (OD600=0.00004). The final DMSO concentration was maintained at 2.5% across all treatments. Following preparation, the plates were incubated at 37°C for 48 hrs and photos were taken with a Bio-Rad Gel Doc XR+ Imaging System.

Plate assays and growth curves were conducted in minimal media or minimal media supplemented with 1 mM ethanolamine (ETA). Wildtype SC5314 and *cho1*ΔΔ strains were grown in YPD overnight and washed three times with H_2O before inoculation. The starting OD_{600} is 0.05 for both plate assays and growth curves. For plate assays, both wildtype and *cho1*ΔΔ strains were grown in flat-bottom 96-well plates at a final volume of 200 μL, in the presence of different compounds or DMSO as indicated at 30°C. The final DMSO concentration was maintained at 2.5 % across all treatments. A Leica inverted microscope was then used to visualize growth after 24-hour incubations. In the meantime, cells grown in different compounds were subjected to live cell counting. Cell cultures from flat-bottom 96-well plates after 24-hour incubation were diluted 100 to 10,000 times before plating on the minimal media, and the total colony forming unit (CFU) was kept within 200 for each plate. A total of six biological replicates were done in each condition.

643 The growth curves with LOC14 and CBR-5884 treatments were measured from 2
644 to 30 hours with OD_{600} measurements every two hours. A final concentration of 170 μM
645 CBR-5884, 430 μM LOC14 and 5 mM serine was added into each group as indicated. To
646 test the stability of CBR-5884, minimal medium supplemented with 170 μM CBR-5884
647 or equivalent DMSO was agitated for 12 hrs before the introduction of wildtype *C.*
648 *albicans* SC5314 strain, and growth curves were recorded from 0 to 14 hrs with OD_{600}
649 measurement every 2hrs. To check the resistance of *C. albicans* in CBR-5884, SC5314
650 strain was grown in 170 μM CBR-5884 for 12 hrs and 24 hrs before being diluted in
651 fresh minimal medium supplemented with fresh 170 μM CBR-5884 or equivalent
652 DMSO. The growth curves were recorded from 0 to 14 hrs with OD_{600} measurement
653 every 2hrs. The final DMSO concentration was maintained at 1.7 % across all treatments.

654 **PS synthase assay**

655 Enzymatic activity of Cho1 in the presence of the compounds was measured using
656 the radioactive PS synthase assay. For purified Cho1, the procedure was fully described
657 in (33). Briefly, 1-2 μg of purified Cho1 was added to the reaction containing 50 mM
658 Tris-HCl (pH = 8.0), 1 mM $MnCl_2$, 0.1% Triton X-100, 0.04% digitonin, 0.1 mM (4.7
659 mol %) 16:0 CDP-DAG (Avanti, cat# 870510) and 0.5 mM L-serine (spiked with 5% (by
660 volume) L-[^{3}H]-serine (15 Ci/mmol)) at a total volume of 100 μL, in the presence of 100
661 μM of each compound or equivalent DMSO solvent. The reaction was conducted at
662 30 °C for 30 min and [^{3}H]PS produced in the reaction was measured using a liquid
663 scintillation counter. For crude membrane samples, crude membrane preps from wildtype
664 and *cho1*ΔΔ strains were collected and assayed as described in (33) with the exception

665 that 2 mM L-serine (spiked with 5% (by volume) L-[^{3}H]-serine (15 Ci/mmol)) was used
666 in each reaction. A final concentration of 1 mM of each compound was used for the crude
667 membrane samples.

668 For CBR-5884 washout assays, purified Cho1 was incubated with CBR-5884 at a
669 final concentration of 100 μM, or equivalent DMSO, in 100 μL volume on ice for 2 hrs.
670 The CBR-5884 was then washed out by exchanging with 4 ml 50 mM Tris-HCl at pH 8.0
671 and 0.1% digitonin three times in the Amicon Ultra Centrifugal Filter (10 kDa MWCO).
672 The sample was concentrated to the volume of approximately 500 μL, and protein
673 concentration was determined using the Pierce detergent-compatible Bradford assay kit.
674 The reaction was set up with 50 mM Tris-HCl (pH = 8.0), 1 mM $MnCl_2$, 0.1% Triton X-
675 100, 0.1% digitonin, 0.1 mM (4.7 mol %) 16:0 CDP-DAG (Avanti, cat# 870510) and 10
676 mM L-serine (spiked with 5% (by volume) L-[3H]-serine (15 Ci/mmol)) at a total
677 volume of 100 μL, in the presence of 100 μM CBR-5884 or equivalent DMSO solvent.
678 The reaction was stopped at 20, 40 and 60 min, and specific activity was calculated based
679 on the slope of linear PS production, representing the initial velocity.

680 For the kinetic curves, the specific activity was measured in the reaction
681 containing 50 mM Tris-HCl (pH = 8.0), 1 mM $MnCl_2$, 0.025-0.3% Triton X-100 and
682 0.033-0.07% digitonin with 0.75 to 1.5 μg purified Cho1 protein. The concentrations of
683 18:1 CDP-DAG (Avanti, cat# 870520) and serine are indicated in the graphs, and the
684 mol % of CDP-DAG was kept between 4.2 – 5.0% for the curve where CDP-DAG was
685 varied (Figure 6C & 6D) and at 4.8% (200 μM) for the curve where serine was varied
686 (Figure 6B). The concentrations of CBR-5884 used in each reaction are indicated in the

687 graph, and CBR-5884 was incubated with purified Cho1 protein on ice for at least 2
688 hours before the addition of L-[^{3}H]-serine. The reaction was stopped at 20, 40 and 60
689 min, and specific activity was calculated based on the slope of linear PS production,
690 representing the initial velocity.

691 **Thin layer chromatography**

692 Wildtype SC5314 and *cho1*ΔΔ strains grown overnight in YPD were inoculated
693 into fresh YPD at OD_{600} of 0.1 and were shaken for another 3 hours. Then, 170 μM CBR-
694 5884 or equivalent DMSO solvent was added to both wildtype and *cho1*ΔΔ cultures, and
695 cells were shaken for another 2 hours. Then, cells were washed with 1xPBS three times
696 and normalized to a total OD_{600} of 1. The phospholipids were extracted with the hot
697 ethanol method as described in (14). A Whatman 250 μm silica gel aluminum backed
698 plate was treated, and separation of phospholipids was carried out as described in (99).
699 Phospholipid standards PI, PE, PS and PC were purchased from Avanti. The
700 quantification of the phospholipids was done in ImageJ software.

701

702

703 **Computational docking**

704 The computational docking was conducted in Molecular Operating Environment
705 software (MOE, Chemical Computing Group, Ltd, Montreal, Canada). A CDP-DAG-
706 bound *C. albicans* Cho1 structure was generated by superposing the *C. albicans* Cho1

AlphaFold model on the CDP-DAG-bound PS synthase from *Methanocaldococcus jannaschii* (PDB: 7B1L) (32). Structures from CBR-5884 and serine were introduced into the structure, and the system was quickly prepped and energy-minimized for docking. Potential docking sites were predicted by "site finder" function in MOE and all the sites having above 0 possibilities are combined for docking (Figure S5B). Both serine and CBR-5884 molecules were docked into the potential sites 20,000 times, and triangle matcher placement (scored by London dG) and rigid receptor refinement (scored by GBVI/WSA dG) were used to pick the top five poses. The ligand interaction map was also generated in MOE.

Statistical analysis and molecular weight (MW) estimation on the gels

All the statistical analyses were performed with GraphPad Prism 9.1 software. The PS synthase activities were compared using ordinary (equal SDs) or Brown-Forsythe and Welch ANOVA tests (unequal SDs). Blue native PAGE and Coomassie Blue R-250 staining were conducted as described in (33) and all MW estimates were conducted in the band analysis tool of the Quantity One software (Bio-Rad).

Data availability

The original contributions presented in the study are included in the manuscript/supplementary files; Source data files have been provided for figures and supplemental figures. Further inquiries can be directed to the corresponding author.

Acknowledgments

The authors would like to thank Dr. Glen E. Palmer and Dr. Brian M. Peters from the University of Tennessee Health Science Center for their pKE4 and *CaHygB*-flipper plasmids. Reese Saho, a summer undergraduate student from Ohio Northern University, also helped with setting up the PS synthase assay. We also thank him for his work.

Author contributions

Conceived and designed the experiments: YZ, GAP, JMR, REL, TBR. Performed the experiments: YZ, GAP, MMM, JM, JMR, EKP, JL, CFA. Analyzed the data: YZ, GAP, TBR. Contributed reagents/materials/analysis tools: JMR, REL, MDB, TBR. Wrote the original draft: YZ. Writing & Editing: YZ, GAP, PMO, CFA, TBR. All authors contributed to the article and approved the submitted version.

Reference

1. Morrell M, Fraser VJ, Kollef MH. 2005. Delaying the empiric treatment of Candida bloodstream infection until positive blood culture results are obtained: a potential risk factor for hospital mortality. Antimicrobial agents and chemotherapy 49:3640-3645.
2. Wisplinghoff H, Bischoff T, Tallent SM, Seifert H, Wenzel RP, Edmond MB. 2004. Nosocomial bloodstream infections in US hospitals: analysis of 24,179 cases from a prospective nationwide surveillance study. Clinical infectious diseases 39:309-317.
3. Patel PK, Erlandsen JE, Kirkpatrick WR, Berg DK, Westbrook SD, Louden C, Cornell JE, Thompson GR, Vallor AC, Wickes BL. 2012. The changing epidemiology of oropharyngeal candidiasis in patients with HIV/AIDS in the era of antiretroviral therapy. AIDS research and treatment 2012.
4. Benedict K, Singleton AL, Jackson BR, Molinari NAM. 2022. Survey of incidence, lifetime prevalence, and treatment of self-reported vulvovaginal candidiasis, United States, 2020. BMC Women's Health 22:147.
5. Novosad SA, Fike L, Dudeck MA, Allen-Bridson K, Edwards JR, Edens C, Sinkowitz-Cochran R, Powell K, Kuhar D. 2020. Pathogens causing central-line–associated bloodstream infections in acute-care hospitals—United States, 2011–2017. Infection Control & Hospital Epidemiology 41:313-319.
6. Brown GD, Denning DW, Gow NA, Levitz SM, Netea MG, White TC. 2012. Hidden killers: human fungal infections. Sci Transl Med 4:165rv13.

7. Bustamante CI. 2005. Treatment of Candida infection: a view from the trenches! Current opinion in infectious diseases 18:490-495.
8. Kullberg B, Filler S, Calderone R. 2002. Candida and candidiasis. ASM Press, Washington, DC.
9. Gow NA, Johnson C, Berman J, Coste AT, Cuomo CA, Perlin DS, Bicanic T, Harrison TS, Wiederhold N, Bromley M. 2022. The importance of antimicrobial resistance in medical mycology. Nature communications 13:5352.
10. Pfaller M, Neofytos D, Diekema D, Azie N, Meier-Kriesche H-U, Quan S-P, Horn D. 2012. Epidemiology and outcomes of candidemia in 3648 patients: data from the Prospective Antifungal Therapy (PATH Alliance®) registry, 2004–2008. Diagnostic microbiology and infectious disease 74:323-331.
11. Holeman Jr CW, Einstein H. 1963. The toxic effects of amphotericin B in man. California medicine 99:90.
12. Ghannoum MA, Rice LB. 1999. Antifungal Agents: Mode of Action, Mechanisms of Resistance, and Correlation of These Mechanisms with Bacterial Resistance. Clinical Microbiology Reviews 12:501-517.
13. Whaley SG, Berkow EL, Rybak JM, Nishimoto AT, Barker KS, Rogers PD. 2016. Azole Antifungal Resistance in Candida albicans and Emerging Non-albicans Candida Species. Front Microbiol 7:2173.
14. Chen YL, Montedonico AE, Kauffman S, Dunlap JR, Menn FM, Reynolds TB. 2010. Phosphatidylserine synthase and phosphatidylserine decarboxylase are essential for cell wall integrity and virulence in Candida albicans. Mol Microbiol 75:1112-32.
15. Davis SE, Tams RN, Solis NV, Wagner AS, Chen T, Jackson JW, Hasim S, Montedonico AE, Dinsmore J, Sparer TE. 2018. Candida albicans cannot acquire sufficient ethanolamine from the host to support virulence in the absence of de novo phosphatidylethanolamine synthesis. Infection and immunity 86:e00815-17.
16. Konarzewska P, Wang Y, Han G-S, Goh KJ, Gao Y-G, Carman GM, Xue C. 2019. Phosphatidylserine synthesis is essential for viability of the human fungal pathogen Cryptococcus neoformans. The Journal of biological chemistry 294:2329-2339.
17. Braun BR, van Het Hoog M, d'Enfert C, Martchenko M, Dungan J, Kuo A, Inglis DO, Uhl MA, Hogues H, Berriman M, Lorenz M, Levitin A, Oberholzer U, Bachewich C, Harcus D, Marcil A, Dignard D, Iouk T, Zito R, Frangeul L, Tekaia F, Rutherford K, Wang E, Munro CA, Bates S, Gow NA, Hoyer LL, Kohler G, Morschhauser J, Newport G, Znaidi S, Raymond M, Turcotte B, Sherlock G, Costanzo M, Ihmels J, Berman J, Sanglard D, Agabian N, Mitchell AP, Johnson AD, Whiteway M, Nantel A. 2005. A human-curated annotation of the Candida albicans genome. PLoS Genet 1:36-57.
18. Kohlwein SD, Kuchler K, Sperka-Gottlieb C, Henry SA, Paltauf F. 1988. Identification of mitochondrial and microsomal phosphatidylserine synthase in Saccharomyces cerevisiae as the gene product of the CHO1 structural gene. J Bacteriol 170:3778-81.
19. Kuchler K, Daum G, Paltauf F. 1986. Subcellular and submitochondrial localization of phospholipid-synthesizing enzymes in Saccharomyces cerevisiae. J Bacteriol 165:901-10.

20. Gaigg B, Simbeni R, Hrastnik C, Paltauf F, Daum G. 1995. Characterization of a microsomal subfraction associated with mitochondria of the yeast, Saccharomyces cerevisiae. Involvement in synthesis and import of phospholipids into mitochondria. Biochimica Et Biophysica Acta (BBA)-Biomembranes 1234:214-220.
21. Poole MA, Homann MJ, Bae-Lee MS, Carman GM. 1986. Regulation of phosphatidylserine synthase from Saccharomyces cerevisiae by phospholipid precursors. Journal of Bacteriology 168:668-672.
22. Carson MA, Atkinson KD, Waechter CJ. 1982. Properties of particulate and solubilized phosphatidylserine synthase activity from Saccharomyces cerevisiae. Inhibitory effect of choline in the growth medium. Journal of Biological Chemistry 257:8115-21.
23. Letts VA, Henry SA. 1985. Regulation of phospholipid synthesis in phosphatidylserine synthase-deficient (chol) mutants of Saccharomyces cerevisiae. J Bacteriol 163:560-7.
24. Letts VA, Klig LS, Bae-Lee M, Carman GM, Henry SA. 1983. Isolation of the yeast structural gene for the membrane-associated enzyme phosphatidylserine synthase. Proceedings of the National Academy of Sciences 80:7279-7283.
25. Bae-Lee MS, Carman GM. 1984. Phosphatidylserine synthesis in Saccharomyces cerevisiae. Purification and characterization of membrane-associated phosphatidylserine synthase. J Biol Chem 259:10857-62.
26. Zhou Y, Cassilly CD, Reynolds TB. 2021. Mapping the Substrate-Binding Sites in the Phosphatidylserine Synthase in Candida albicans. Frontiers in Cellular and Infection Microbiology 11.
27. Nikawa J, Tsukagoshi Y, Kodaki T, Yamashita S. 1987. Nucleotide sequence and characterization of the yeast PSS gene encoding phosphatidylserine synthase. Eur J Biochem 167:7-12.
28. Hjelmstad RH, Bell RM. 1991. sn-1,2-diacylglycerol choline- and ethanolaminephosphotransferases in Saccharomyces cerevisiae. Nucleotide sequence of the EPT1 gene and comparison of the CPT1 and EPT1 gene products. J Biol Chem 266:5094-103.
29. Hjelmstad RH, Bell RM. 1990. The sn-1,2-diacylglycerol cholinephosphotransferase of Saccharomyces cerevisiae. Nucleotide sequence, transcriptional mapping, and gene product analysis of the CPT1 gene. J Biol Chem 265:1755-64.
30. Grāve K, Bennett MD, Högbom M. 2019. Structure of Mycobacterium tuberculosis phosphatidylinositol phosphate synthase reveals mechanism of substrate binding and metal catalysis. Communications Biology 2:175.
31. Zhou Y, Reynolds T. 2021. Identification of the substrate-binding sites in the phosphatidylserine synthase from Candida albicans. The FASEB Journal 35.
32. Centola M, van Pee K, Betz H, Yildiz Ö. 2021. Crystal structures of phosphatidyl serine synthase PSS reveal the catalytic mechanism of CDP-DAG alcohol O-phosphatidyl transferases. Nature Communications 12:6982.
33. Zhou Y, Syed JH, Semchonok DA, Wright E, Kyrilis FL, Hamdi F, Kastritis PL, Bruce BD, Reynolds TB. 2023. Solubilization, purification, and characterization

of the hexameric form of phosphatidylserine synthase from Candida albicans. Journal of Biological Chemistry 299.
34. Nogly P, Gushchin I, Remeeva A, Esteves AM, Borges N, Ma P, Ishchenko A, Grudinin S, Round E, Moraes I, Borshchevskiy V, Santos H, Gordeliy V, Archer M. 2014. X-ray structure of a CDP-alcohol phosphatidyltransferase membrane enzyme and insights into its catalytic mechanism. Nat Commun 5:4169.
35. Sciara G, Clarke OB, Tomasek D, Kloss B, Tabuso S, Byfield R, Cohn R, Banerjee S, Rajashankar KR, Slavkovic V, Graziano JH, Shapiro L, Mancia F. 2014. Structural basis for catalysis in a CDP-alcohol phosphotransferase. Nat Commun 5:4068.
36. Clarke OB, Tomasek D, Jorge CD, Dufrisne MB, Kim M, Banerjee S, Rajashankar KR, Shapiro L, Hendrickson WA, Santos H, Mancia F. 2015. Structural basis for phosphatidylinositol-phosphate biosynthesis. Nat Commun 6:8505.
37. Dufrisne MB, Jorge CD, Timóteo CG, Petrou VI, Ashraf KU, Banerjee S, Clarke OB, Santos H, Mancia F. 2020. Structural and Functional Characterization of Phosphatidylinositol-Phosphate Biosynthesis in Mycobacteria. Journal of Molecular Biology.
38. Wang L, Zhou M. 2023. Structure of a eukaryotic cholinephosphotransferase-1 reveals mechanisms of substrate recognition and catalysis. Nature Communications 14:2753.
39. Wang Z, Yang M, Yang Y, He Y, Qian H. 2023. Structural basis for catalysis of human choline/ethanolamine phosphotransferase 1. Nature Communications 14:2529.
40. Yang B, Yao H, Li D, Liu Z. 2021. The phosphatidylglycerol phosphate synthase PgsA utilizes a trifurcated amphipathic cavity for catalysis at the membrane-cytosol interface. Current Research in Structural Biology 3:312-323.
41. Nikawa J-I, Yamashita S. 1981. Characterization of phosphatidylserine synthase from saccharomyces cerevisiae and a mutant defective in the enzyme. Biochimica et Biophysica Acta (BBA) - Lipids and Lipid Metabolism 665:420-426.
42. Carman GM, Matas J. 1981. Solubilization of microsomal-associated phosphatidylserine synthase and phosphatidylinositol synthase from Saccharomyces cerevisiae. Can J Microbiol 27:1140-9.
43. KIYONO K, MIURA K, KUSHIMA Y, HIKIJI T, FUKUSHIMA M, SHIBUYA I, OHTA A. 1987. Primary Structure and Product Characterization of the Saccharomyces cerevisiae CHO1 Gene That Encodes Phosphatidylserine Synthase1. The Journal of Biochemistry 102:1089-1100.
44. Mandal S, Moudgil Mn, Mandal SK. 2009. Rational drug design. European Journal of Pharmacology 625:90-100.
45. Cassilly CD, Maddox MM, Cherian PT, Bowling JJ, Hamann MT, Lee RE, Reynolds TB. 2016. SB-224289 Antagonizes the Antifungal Mechanism of the Marine Depsipeptide Papuamide A. PLoS One 11:e0154932.
46. Pokharel M, Konarzewska P, Roberge JY, Han G-S, Wang Y, Carman GM, Xue C. 2022. The Anticancer Drug Bleomycin Shows Potent Antifungal Activity by Altering Phospholipid Biosynthesis. Microbiology Spectrum 10:e00862-22.

47. Cassilly CD, Farmer AT, Montedonico AE, Smith TK, Campagna SR, Reynolds TB. 2017. Role of phosphatidylserine synthase in shaping the phospholipidome of Candida albicans. FEMS Yeast Res 17.
48. Zhou Y, Bruce B, Reynolds T. 2022. Solubilization and purification of phosphatidylserine synthase from Candida albicans. The FASEB Journal 36.
49. Wu ZL, Ethen CM, Prather B, Machacek M, Jiang W. 2011. Universal phosphatase-coupled glycosyltransferase assay. Glycobiology 21:727-33.
50. Willems HME, Bruner WS, Barker KS, Liu J, Palmer GE, Peters BM. 2017. Overexpression of Candida albicans Secreted Aspartyl Proteinase 2 or 5 Is Not Sufficient for Exacerbation of Immunopathology in a Murine Model of Vaginitis. Infect Immun 85.
51. Lawson KV, Kalisiak J, Lindsey EA, Newcomb ET, Leleti MR, Debien L, Rosen BR, Miles DH, Sharif EU, Jeffrey JL, Tan JBL, Chen A, Zhao S, Xu G, Fu L, Jin L, Park TW, Berry W, Moschütz S, Scaletti E, Sträter N, Walker NP, Young SW, Walters MJ, Schindler U, Powers JP. 2020. Discovery of AB680: A Potent and Selective Inhibitor of CD73. J Med Chem 63:11448-11468.
52. Zhang J-H, Chung TDY, Oldenburg KR. 1999. A Simple Statistical Parameter for Use in Evaluation and Validation of High Throughput Screening Assays. Journal of Biomolecular Screening 4:67-73.
53. Baell JB, Nissink JWM. 2018. Seven Year Itch: Pan-Assay Interference Compounds (PAINS) in 2017—Utility and Limitations. ACS Chemical Biology 13:36-44.
54. Willcox M, Webb B, Thakur A, Harty D. 1998. Interactions between Candida species and platelets. Journal of medical microbiology 47:103-110.
55. Vargas K, Wertz PW, Drake D, Morrow B, Soll DR. 1994. Differences in adhesion of Candida albicans 3153A cells exhibiting switch phenotypes to buccal epithelium and stratum corneum. Infect Immun 62:1328-35.
56. Mullarky E, Lucki NC, Beheshti Zavareh R, Anglin JL, Gomes AP, Nicolay BN, Wong JC, Christen S, Takahashi H, Singh PK, Blenis J, Warren JD, Fendt SM, Asara JM, DeNicola GM, Lyssiotis CA, Lairson LL, Cantley LC. 2016. Identification of a small molecule inhibitor of 3-phosphoglycerate dehydrogenase to target serine biosynthesis in cancers. Proc Natl Acad Sci U S A 113:1778-83.
57. Davis SE, Hopke A, Minkin SC, Montedonico AE, Wheeler RT, Reynolds TB. 2014. Masking of β(1-3)-Glucan in the Cell Wall of Candida albicans from Detection by Innate Immune Cells Depends on Phosphatidylserine. Infection and Immunity 82:4405-4413.
58. Weber RWS. 2002. Vacuoles and the fungal lifestyle. Mycologist 16:10-20.
59. Ancajas CF, Alam S, Alves DS, Zhou Y, Wadsworth NM, Cassilly CD, Ricks TJ, Carr AJ, Reynolds TB, Barrera FN, Best MD. 2023. Cellular Labeling of Phosphatidylserine Using Clickable Serine Probes. ACS Chemical Biology 18:377-384.
60. Ancajas CF, Carr AJ, Lou J, Sagar R, Zhou Y, Reynolds TB, Best MD. 2023. Harnessing Clickable Acylated Glycerol Probes as Chemical Tools for Tracking Glycerolipid Metabolism. Chemistry – A European Journal 29:e202300417.

61. Antonsson BE. 1994. Purification and characterization of phosphatidylinositol synthase from human placenta. Biochemical Journal 297:517-522.
62. Antonioli L, Pacher P, Vizi ES, Haskó G. 2013. CD39 and CD73 in immunity and inflammation. Trends in molecular medicine 19:355-367.
63. Cardoso AM, Schetinger MRC, Correia-de-Sá P, Sévigny J. 2015. Impact of ectonucleotidases in autonomic nervous functions. Autonomic Neuroscience 191:25-38.
64. Duarte-Araújo M, Nascimento C, Timóteo MA, Magalhães-Cardoso MT, Correia-de-Sá P. 2009. Relative contribution of ecto-ATPase and ecto-ATPDase pathways to the biphasic effect of ATP on acetylcholine release from myenteric motoneurons. Br J Pharmacol 156:519-33.
65. Maiorino M, Roveri A, Ursini F. 1992. Antioxidant effect of ebselen (PZ 51): Peroxidase mimetic activity on phospholipid and cholesterol hydroperoxides vs free radical scavenger activity. Archives of Biochemistry and Biophysics 295:404-409.
66. Maiorino M, Roveri A, Coassin M, Ursini F. 1988. Kinetic mechanism and substrate specificity of glutathione peroxidase activity of ebselen (PZ51). Biochem Pharmacol 37:2267-71.
67. Parnham M, Sies H. 2000. Ebselen: prospective therapy for cerebral ischaemia. Expert Opinion on Investigational Drugs 9:607-619.
68. Liang Q, Shen N, Lai B, Xu C, Sun Z, Wang Z, Li S. 2019. Electrical Stimulation Degenerated Cochlear Synapses Through Oxidative Stress in Neonatal Cochlear Explants. Front Neurosci 13:1073.
69. Haritha CV, Sharun K, Jose B. 2020. Ebselen, a new candidate therapeutic against SARS-CoV-2. Int J Surg 84:53-56.
70. Nakamura Y, Feng Q, Kumagai T, Torikai K, Ohigashi H, Osawa T, Noguchi N, Niki E, Uchida K. 2002. Ebselen, a glutathione peroxidase mimetic seleno-organic compound, as a multifunctional antioxidant. Implication for inflammation-associated carcinogenesis. J Biol Chem 277:2687-94.
71. Jin Z, Du X, Xu Y, Deng Y, Liu M, Zhao Y, Zhang B, Li X, Zhang L, Peng C, Duan Y, Yu J, Wang L, Yang K, Liu F, Jiang R, Yang X, You T, Liu X, Yang X, Bai F, Liu H, Liu X, Guddat LW, Xu W, Xiao G, Qin C, Shi Z, Jiang H, Rao Z, Yang H. 2020. Structure of Mpro from SARS-CoV-2 and discovery of its inhibitors. Nature 582:289-293.
72. Venturini TP, Chassot F, Loreto É S, Keller JT, Azevedo MI, Zeni G, Santurio JM, Alves SH. 2016. Antifungal activities of diphenyl diselenide and ebselen alone and in combination with antifungal agents against Fusarium spp. Med Mycol 54:550-5.
73. Thangamani S, Eldesouky HE, Mohammad H, Pascuzzi PE, Avramova L, Hazbun TR, Seleem MN. 2017. Ebselen exerts antifungal activity by regulating glutathione (GSH) and reactive oxygen species (ROS) production in fungal cells. Biochimica et Biophysica Acta (BBA)-General Subjects 1861:3002-3010.
74. Sakita KM, Capoci IRG, Conrado PCV, Rodrigues-Vendramini FAV, Faria DR, Arita GS, Becker TCA, Bonfim-Mendonça PS, Svidzinski TIE, Kioshima ES. 2021. Efficacy of Ebselen Against Invasive Aspergillosis in a Murine Model. Front Cell Infect Microbiol 11:684525.

75. Marshall AC, Kidd SE, Lamont-Friedrich SJ, Arentz G, Hoffmann P, Coad BR, Bruning JB. 2019. Structure, Mechanism, and Inhibition of Aspergillus fumigatus Thioredoxin Reductase. Antimicrob Agents Chemother 63.
76. Marshall MO, Kates M. 1974. Biosynthesis of Nitrogenous Phospholipids in Spinach Leaves. Canadian Journal of Biochemistry 52:469-482.
77. Billack B, Pietka-Ottlik M, Santoro M, Nicholson S, Młochowski J, Lau-Cam C. 2010. Evaluation of the antifungal and plasma membrane H+-ATPase inhibitory action of ebselen and two ebselen analogs in S. cerevisiae cultures. J Enzyme Inhib Med Chem 25:312-7.
78. Chan G, Hardej D, Santoro M, Lau-Cam C, Billack B. 2007. Evaluation of the antimicrobial activity of ebselen: Role of the yeast plasma membrane H+-ATPase. Journal of Biochemical and Molecular Toxicology 21:252-264.
79. Azad GK, Singh V, Mandal P, Singh P, Golla U, Baranwal S, Chauhan S, Tomar RS. 2014. Ebselen induces reactive oxygen species (ROS)-mediated cytotoxicity in Saccharomyces cerevisiae with inhibition of glutamate dehydrogenase being a target. FEBS Open Bio 4:77-89.
80. Azad GK, Balkrishna SJ, Sathish N, Kumar S, Tomar RS. 2012. Multifunctional Ebselen drug functions through the activation of DNA damage response and alterations in nuclear proteins. Biochem Pharmacol 83:296-303.
81. Terentis AC, Freewan M, Sempértegui Plaza TS, Raftery MJ, Stocker R, Thomas SR. 2010. The selenazal drug ebselen potently inhibits indoleamine 2,3-dioxygenase by targeting enzyme cysteine residues. Biochemistry 49:591-600.
82. Kaplan A, Gaschler MM, Dunn DE, Colligan R, Brown LM, Palmer AG, 3rd, Lo DC, Stockwell BR. 2015. Small molecule-induced oxidation of protein disulfide isomerase is neuroprotective. Proc Natl Acad Sci U S A 112:E2245-52.
83. Zhou X, Li G, Kaplan A, Gaschler MM, Zhang X, Hou Z, Jiang M, Zott R, Cremers S, Stockwell BR, Duan W. 2018. Small molecule modulator of protein disulfide isomerase attenuates mutant huntingtin toxicity and inhibits endoplasmic reticulum stress in a mouse model of Huntington's disease. Hum Mol Genet 27:1545-1555.
84. Chamberlain N, Korwin-Mihavics BR, Nakada EM, Bruno SR, Heppner DE, Chapman DG, Hoffman SM, van der Vliet A, Suratt BT, Dienz O, Alcorn JF, Anathy V. 2019. Lung epithelial protein disulfide isomerase A3 (PDIA3) plays an important role in influenza infection, inflammation, and airway mechanics. Redox Biol 22:101129.
85. Chen QX, Liu XD, Huang H. 2003. Inactivation kinetics of mushroom tyrosinase in the dimethyl sulfoxide solution. Biochemistry (Mosc) 68:644-9.
86. Milčić N, Stepanić V, Crnolatac I, Findrik Blažević Z, Brkljača Z, Majerić Elenkov M. 2022. Inhibitory Effect of DMSO on Halohydrin Dehalogenase: Experimental and Computational Insights into the Influence of an Organic Co-solvent on the Structural and Catalytic Properties of a Biocatalyst. Chemistry – A European Journal 28:e202201923.
87. Ostermeier L, Oliva R, Winter R. 2020. The multifaceted effects of DMSO and high hydrostatic pressure on the kinetic constants of hydrolysis reactions catalyzed by α-chymotrypsin. Physical Chemistry Chemical Physics 22:16325-16333.

88. Cassilly CD, Reynolds TB. 2018. PS, It's Complicated: The Roles of Phosphatidylserine and Phosphatidylethanolamine in the Pathogenesis of Candida albicans and Other Microbial Pathogens. J Fungi (Basel) 4.
89. McMaster CR, Bell RM. 1994. Phosphatidylcholine biosynthesis in Saccharomyces cerevisiae. Regulatory insights from studies employing null and chimeric sn-1,2-diacylglycerol choline- and ethanolaminephosphotransferases. J Biol Chem 269:28010-6.
90. Williams JG, McMaster CR. 1998. Scanning alanine mutagenesis of the CDP-alcohol phosphotransferase motif of Saccharomyces cerevisiae cholinephosphotransferase. J Biol Chem 273:13482-7.
91. Paulus H, Kennedy EP. 1960. The enzymatic synthesis of inositol monophosphatide. Journal of Biological Chemistry 235:1303-1311.
92. Fischl AS, Carman GM. 1983. Phosphatidylinositol biosynthesis in Saccharomyces cerevisiae: purification and properties of microsome-associated phosphatidylinositol synthase. Journal of Bacteriology 154:304-311.
93. Liu J, Vogel AK, Miao J, Carnahan JA, Lowes DJ, Rybak JM, Peters BM. 2022. Rapid Hypothesis Testing in Candida albicans Clinical Isolates Using a Cloning-Free, Modular, and Recyclable System for CRISPR-Cas9 Mediated Mutant and Revertant Construction. Microbiol Spectr 10:e0263021.
94. Nishiguchi G, Das S, Ochoada J, Long H, Lee RE, Rankovic Z, Shelat AA. 2021. Evaluating and evolving a screening library in academia: the St Jude approach. Drug Discov Today 26:1060-1069.
95. Canham SM, Wang Y, Cornett A, Auld DS, Baeschlin DK, Patoor M, Skaanderup PR, Honda A, Llamas L, Wendel G. 2020. Systematic chemogenetic library assembly. Cell chemical biology 27:1124-1129.
96. Chen T, Jackson JW, Tams RN, Davis SE, Sparer TE, Reynolds TB. 2019. Exposure of Candida albicans β (1,3)-glucan is promoted by activation of the Cek1 pathway. PLOS Genetics 15:e1007892.
97. Clinical, Institute LS. 2008. Reference method for broth dilution antifungal susceptibility testing of yeasts. Clinical and Laboratory Standards Institute Wayne, PA.
98. Wayne P. 2008. Reference method for broth dilution antifungal susceptibility testing of yeasts. Approved Standard 3:6-12.
99. Vaden DL, Gohil VM, Gu Z, Greenberg ML. 2005. Separation of yeast phospholipids using one-dimensional thin-layer chromatography. Analytical biochemistry 338:162-164.

Figures

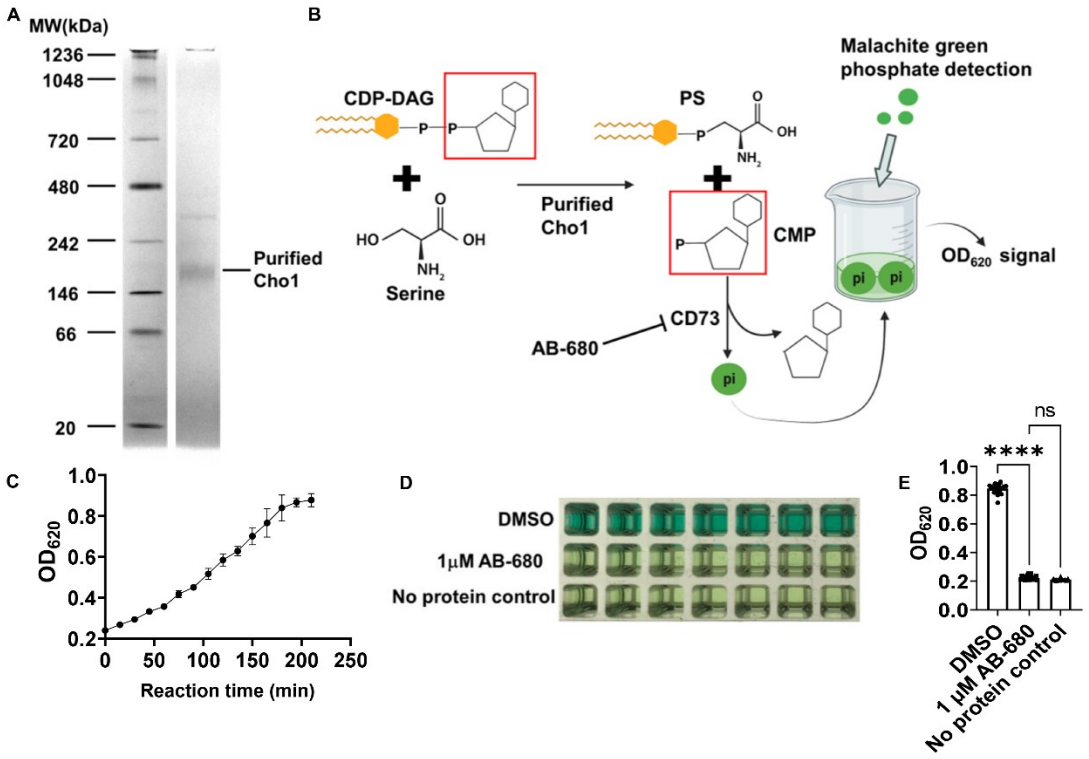

1071

1072 **Figure 1. A malachite-green-based nucleotidase-coupled assay measures the activity**
1073 **of purified Cho1 protein. (A)** Blue native PAGE gel of the purified hexameric tag-free
1074 Cho1 protein. Purified Cho1 and protein ladder with known MW are indicated. The gel
1075 was stained with Coomassie Blue R-250. **(B)** Schematic representation of the malachite-
1076 green-based nucleotidase-couple assay. Cho1 synthesizes PS from CDP-DAG
1077 (cytidyldiphosphate-diacylglycerol) and serine. This releases PS and CMP
1078 (cytidylmonophosphate). The phosphate from CMP is cleaved by the nucleotidase CD73
1079 to release inorganic phosphate, which can be bound by the malachite green reagent and
1080 measured colorimetrically at OD_{620}. AB-680 is a potent inhibitor of CD73, and can thus
1081 inhibit the reaction. **(C)** OD_{620} signal from the malachite green reagent that was added to
1082 the reaction shown in **(B)** at different time points after the reaction started. Reactions
1083 were set up with the same conditions and stopped by adding malachite green at the time

indicated. The dots represent the mean of four biological replicates, and the error bars are ± standard deviation (S.D.) values. **(D)** Inhibition of the nucleotidase-coupled assay by AB-680 is shown for a series of replicates in 384-well format and **(E)** is quantified for a total of 21 replicates. Statistics were conducted using one-way ANOVA using Tukey's multiple comparisons test (ns=not significant, ****, $p < 0.0001$).

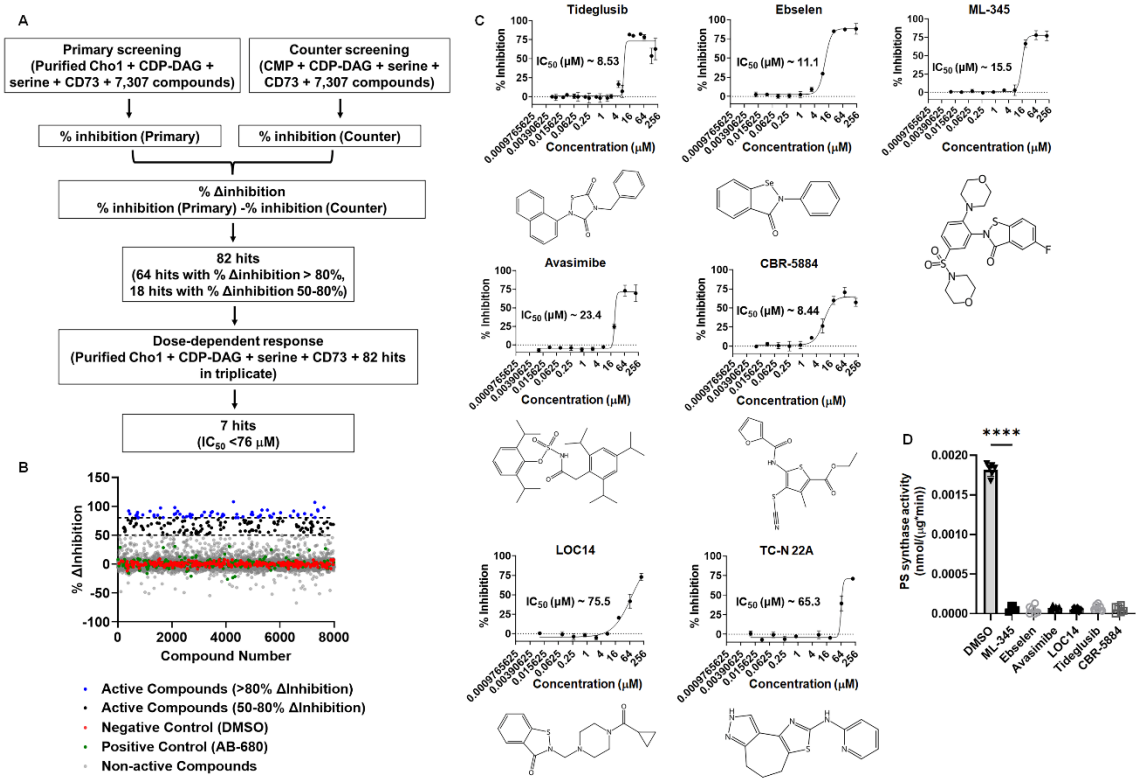

Figure 2. Seven Cho1-specific inhibitors were identified from the high-throughput malachite green screen. (A) Flowchart for the primary and counter screen and the calculation of % Δinhibition. **(B)** The dot plot of % Δinhibition for all the compounds, including controls, used in the screen. Reaction with DMSO and AB-680 were used as 0% Δinhibition (negative) and 100% Δinhibition (positive) controls, respectively. The two dotted lines from the Y-axis indicate 80 and 50% Δinhibition, respectively. **(C)**

Dose-response curve and structure of the seven non-pan-assay interference (non-PAINS) compounds identified from the screen. The dots represent the mean of three replicates, and the error bars are ± standard deviation (S.D.) values. Best-fit IC_{50} values (in μM) were shown in each graph. **(D)** The PS synthase activity of purified Cho1 was measured by L-[^{3}H]-serine incorporation into PS in the presence of different inhibitors at 100 μM or equivalent DMSO, and are presented as nmol/(μg protein*min). Statistics were conducted using one-way ANOVA and Dunnett's T3 multiple comparisons test (****, 0.0001> p). The activities were measured in duplicate with a total of six biological replicates as indicated. The bars represent the mean and the error bars are ± S.D. values.

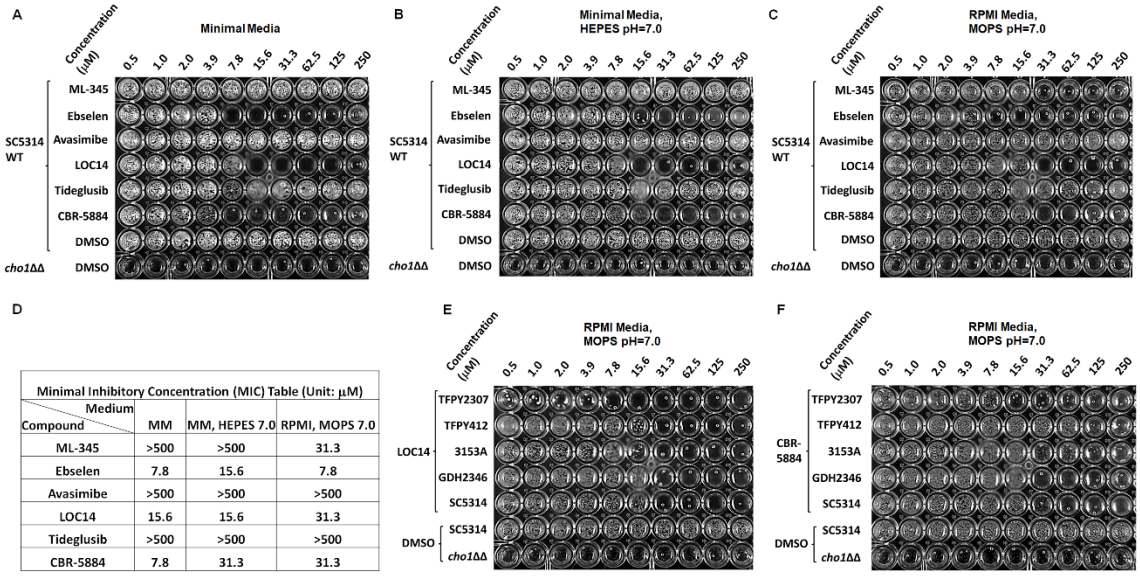

Minimal Inhibitory Concentration (MIC) Table (Unit: μM)

Compound \ Medium	MM	MM, HEPES 7.0	RPMI, MOPS 7.0
ML-345	>500	>500	31.3
Ebselen	7.8	15.6	7.8
Avasimibe	>500	>500	>500
LOC14	15.6	15.6	31.3
Tideglusib	>500	>500	>500
CBR-5884	7.8	31.3	31.3

Figure 3. Ebselen, LOC14 and CBR-5884 inhibited cell growth of *C. albicans* in different media. (A-C) The MIC was measured for each compound in three different media for 48 hours: minimal medium **(A)**, minimal medium buffered with 50 mM HEPES (pH=7.0) **(B)**, and RPMI MOPS (pH=7.0) **(C)**. These tests were conducted, by

standard CLSI MIC broth microdilution protocols, against the wildtype SC5314 strain, using DMSO as a negative control, and against the *cho1*ΔΔ mutant with DMSO serving as a positive control. **(D)** A summary table of all MIC values from **(A-C)**. **(E-F)** Multiple wildtype *C. albicans* isolates were tested with different concentrations of LOC14 **(E)** and CBR-5884 **(F).** All concentrations indicated are micromolar (μM).

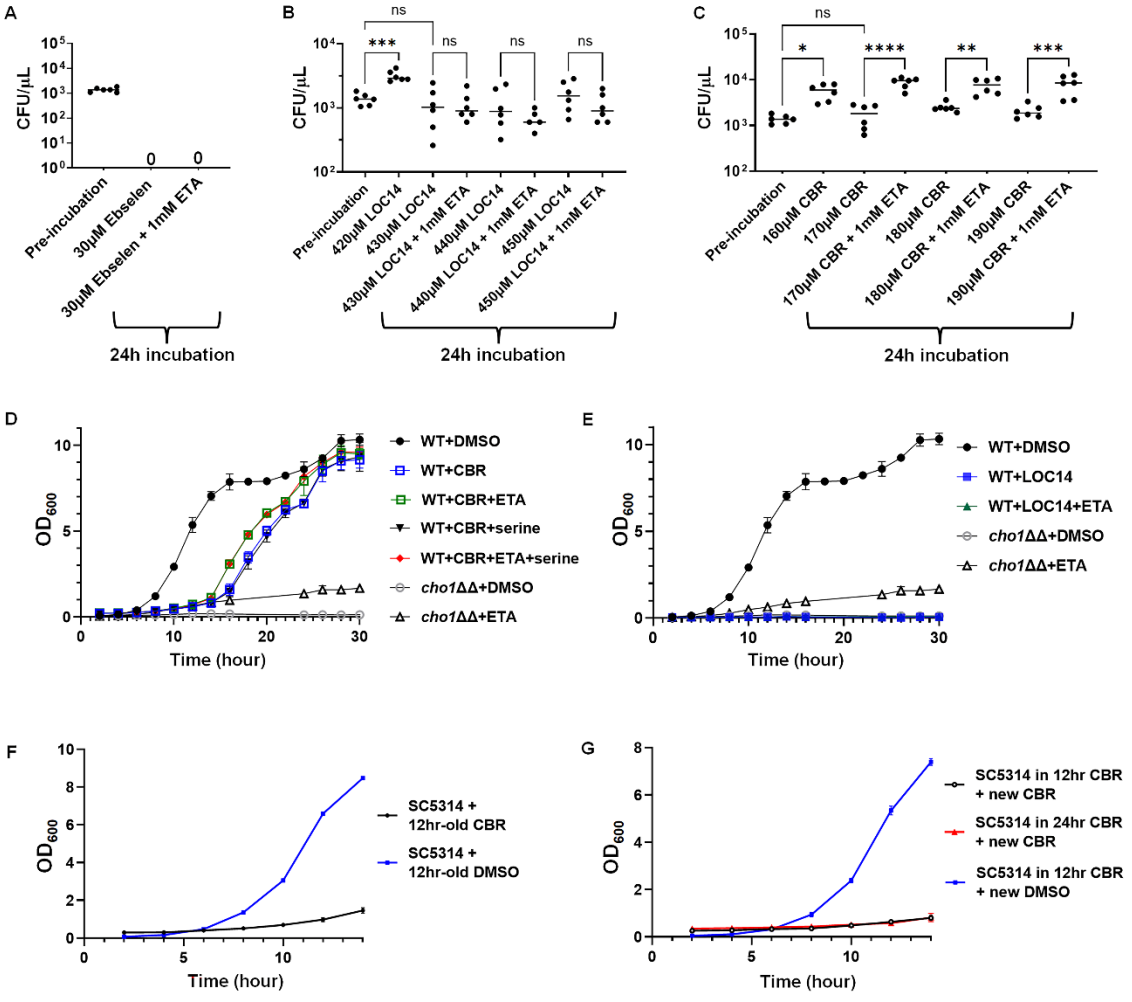

Figure 4. Ethanolamine supplementation can mitigate the inhibitory effects of CBR-5884. (A-C) Colony forming units (CFUs) from cells treated with different concentrations of **(A)** ebselen, **(B)** LOC14 and **(C)** CBR-5884, ± 1 mM ethanolamine

(ETA), for 24 hours compared to pre-incubation. Statistics were conducted using one-way ANOVA and Tukey's multiple comparisons test (ns=not significant, $p > 0.05$; *, $0.05 > p > 0.01$, **, $0.01 > p > 0.001$). Six biological replicates were tested in each treatment. **(D)** Growth curves of wildtype *C. albicans* in the presence of 170 μM CBR-5884 or equivalent DMSO, with the addition of 1 mM ethanolamine (ETA) or 5 mM serine or both, from 0 to 30 hrs. The *cho1*ΔΔ strain was also included as a control. **(E)** Growth curves of wildtype *C. albicans* in the presence of 430 μM LOC-5884 or equivalent DMSO, with the addition of 1 mM ethanolamine (ETA), from 0 to 30 hrs. **(F)** Minimal medium supplemented with 170 μM CBR-5884 or equivalent DMSO was agitated for 12 hrs before the introduction of wildtype *C. albicans* SC5314 strain, and growth curves were recorded from 0 to 14 hrs. **(G)** Wildtype *C. albicans* SC5314 strain was grown in 170 μM CBR-5884 for 12 hrs and 24 hrs before being diluted in fresh minimal medium supplemented with 170 μM CBR-5884 or equivalent DMSO. The growth curves were recorded from 0 to 14 hrs. The dots in **(D-G)** represent the mean values of six biological replicates, and the error bars are ± standard deviation (S.D.) values.

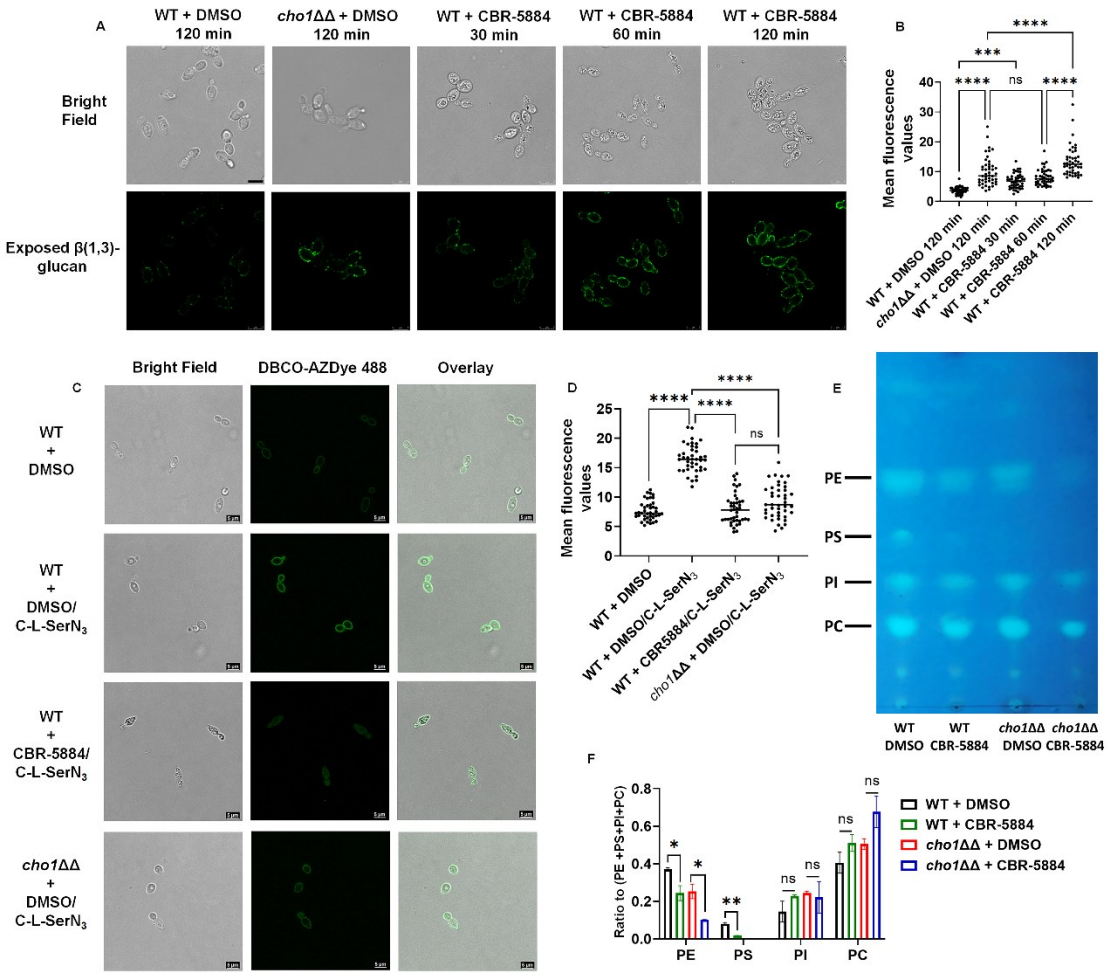

Figure 5. CBR-5884 interferes with *in vivo* PS synthesis. (A) CBR-5884 induces cell wall β(1,3)-glucan exposure. Exposure of cell wall β(1,3)-glucan by wildtype *C. albicans* treated with 170 μM CBR-5884 or equivalent DMSO control was measured at the indicated time points. Exposed β(1,3)-glucan is shown as green fluorescence and the corresponding bright field images are shown. **(B)** Quantification of the mean fluorescence from **(A)**. Forty-six cells from at least 10 fields of view were used for the quantification for each condition. Statistics were conducted using one-way ANOVA and Tukey's multiple comparisons test (ns=not significant, $p > 0.05$; ****, $0.0001 > p$). **(C)** CBR-5884 interferes with the incorporation of C-L-SerN$_3$ probe into the cell membrane. A final concentration of 1.5 mM C-L-SerN$_3$ was added to wildtype *C. albicans* and *cho1*ΔΔ cells

grown with and without 170 μM CBR-5884. The cells were then stained with the DBCO-AZ Dye 488 to allow click-tagging, followed by microscopy. Corresponding brightfield and overlay images were also shown. Wildtype *C. albicans* grown without the C-L-SerN_3 probe was included as a control for background fluorescence. **(D)** Quantification of the mean fluorescence from **(C)**. Forty cells from at least 10 fields of view for each condition were used for the quantification. Statistics were conducted using one-way ANOVA and Tukey's multiple comparisons test (ns=not significant, $p > 0.05$; ****, $0.0001 > p$). **(E)** Thin layer chromatography (TLC) plate of phospholipids extracted from wildtype and *cho1*ΔΔ *C. albicans* treated with 170 μM CBR-5884 or equivalent DMSO. The positions of PS (phosphatidylserine), PE (phosphatidylethanolamine), PI (phosphatidylinositol) and PC (phosphatidylcholine) are indicated based on standards. **(F)** The ratio of the phospholipid to total (PE+PS+PI+PC) phospholipids for strains in **(E)**. The quantification was done in ImageJ software from two TLC plates. Statistics were conducted using unpaired two-tailed t test (ns=not significant, $p > 0.05$; *, $0.05 > p > 0.01$, **, $0.01 > p > 0.001$).

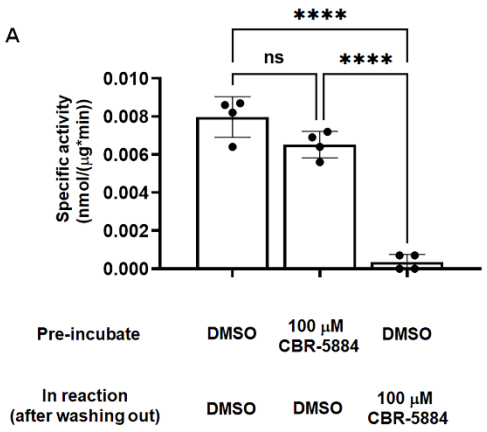

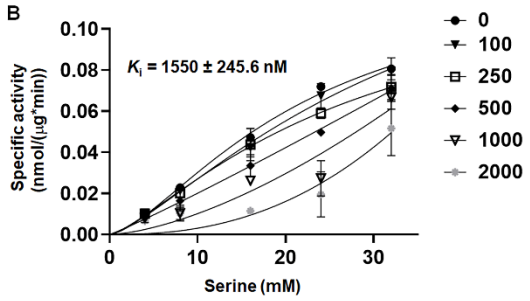

Model comparison	Probability		Preferred model
	Former	Latter	
Competitive inhibition vs. Noncompetitive inhibition	74.58%	25.42%	Competitive
Competitive inhibition vs. Uncompetitive inhibition	>99.99%	<0.01%	Competitive

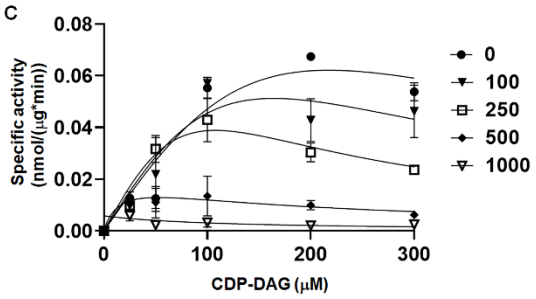

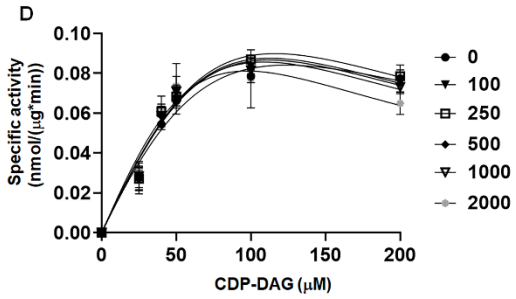

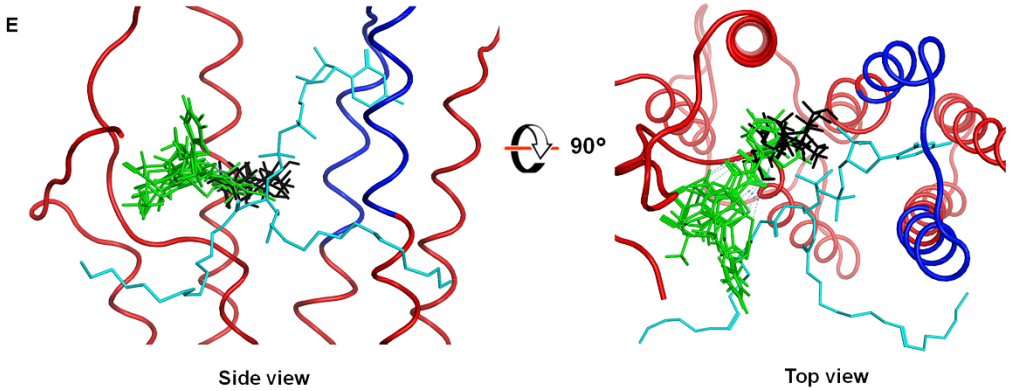

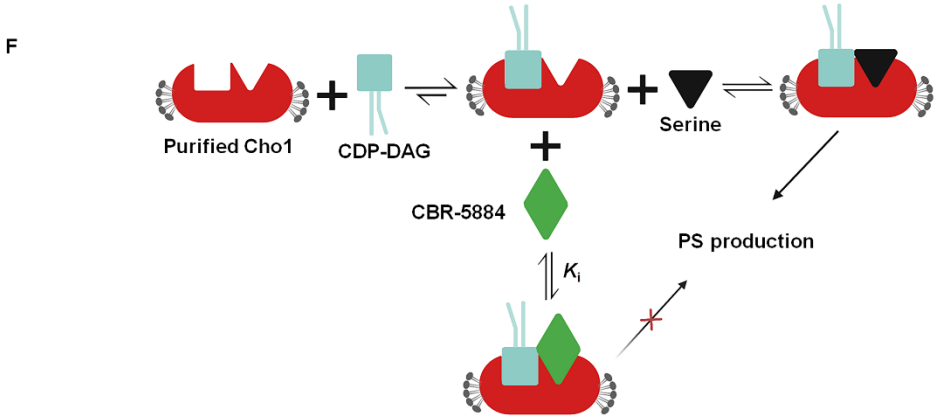

1166

Figure 6. CBR-5884 may function as a competitive inhibitor occupying the serine binding site of Cho1. (A) Purified Cho1 was pre-incubated with DMSO or 100 μM CBR-5884 for 2 hrs before being washed out and tested against DMSO or 100 μM CBR-5884. Four specific activities were measured for each condition and statistics were conducted using one-way ANOVA and Tukey's multiple comparisons test (****, 0.0001> p). **(B)** Kinetic curves for serine in the presence of CBR-5884. CDP-DAG was kept constant at 200 μM (4.8 mol %, K_m = 36.66 ± 11.10 μM), and the specific activities of purified hexameric Cho1 were plotted against various serine concentrations (4, 8, 16, 24, 32 mM) in the presence of 0, 100, 250, 500, 1000, 2000 nM CBR-5884. The curves best fit for competitive inhibition with a K_i value of 1550 ± 245.6 nM. The dots in all curves represent the mean values of two biological replicates, and the error bars are ± standard deviation (S.D.) values. **(C)** Kinetic curves for CDP-DAG in the presence of CBR-5884. Serine was kept constant at 20 mM (K_{half} = 17.08 ± 4.072 mM), and the specific activities of purified hexameric Cho1 were plotted against various CDP-DAG concentrations (25, 50, 100, 200, 300 μM, 4.2 – 5.0 mol %) in the presence of 0, 100, 250, 500 and 1000 nM CBR-5884. **(D)** Kinetic curves for CDP-DAG in the presence of CBR-5884 with 32 mM serine (K_{half} = 17.08 ± 4.072 mM). Specific activities of purified hexameric Cho1 were plotted against various CDP-DAG concentrations in the presence of 0, 100, 250, 500, 1000 and 2000 nM CBR-5884. **(E)** Computational docking of serine and CBR-5884 into the Cho1 AlphaFold structure. The top 5 poses of CBR-5884 (green) and serine (black) are shown within the active site of Cho1. CDP-DAG is shown as cyan and the conserved CAPT motif of Cho1 is highlighted in dark blue. **(F)** A model for the inhibition mechanism of CBR-5884 to Cho1. Cho1 follows a sequential bi-bi reaction, in

1190 which it has to bind CDP-DAG prior to serine for catalysis. In the presence of CBR-
1191 5884, CDP-DAG-bound Cho1 could either bind serine for a reaction or CBR-5884 for no
1192 reaction.

1193